Thermodynamic Modeling of Phase and Tension Behavior of CO_2/Hydrocarbon Systems

Muhammad Sahimi,* U. of Minnesota
H. Ted Davis, SPE, U. of Minnesota
L.E. Scriven, SPE, U. of Minnesota

Abstract

The gradient theory of inhomogeneous fluid is used to predict phase splits and compositions, interfacial composition profiles, and interfacial tension (IFT) of liquid-liquid, liquid-vapor, and liquid-liquid-vapor equilibria in binary and ternary mixtures of CO_2 with propane and decane. The theory's input are the equation of state (EOS) of homogeneous fluid and the influence parameters of inhomogeneous fluid. An efficient computational algorithm is presented for simultaneously generating phase behavior, critical points, interfacial composition profiles, and tension between the phases. Most calculations are made with the Peng-Robinson EOS and the geometric mixing rule for the influence parameters. Use of other EOS and alternative schemes for choosing the influence parameters is explored.

Introduction

CO_2 is a promising agent for enhancing petroleum recovery. Laboratory and field studies have established that CO_2 can be an efficient oil-displacing agent.[1-4] The various mechanisms by which it can act include (1) solution gas drive, (2) immiscible CO_2 drive, (3) hydrocarbon/CO_2 miscible drive, (4) hydrocarbon vaporization, (5) direct miscible CO_2 drive, and (6) multicontact dynamic miscible drive.[5] Phase-equilibria data for CO_2-reservoir oils have been reported.[6,7] The data suggest that two distinct types of equilibria are possible. In one, there are only two phases, liquid and vapor. In the other, there is a region of liquid-vapor equilibrium, but in the phase diagram it exists in conjunction with both liquid-liquid and liquid-liquid-vapor regions.[7]

Hutchinson and Braun[8] have shown how a lean gas can develop miscibility with a relatively rich oil. Miscibility is achieved when the lean gas strips intermediates from the liquid until the gas composition is rich enough to be miscible with the original oil. This process is called the high-pressure or vaporizing gas drive. In CO_2/crude-oil systems of only one liquid phase and one vapor phase, the miscibility development mechanism can be regarded as vaporization.[9] If the temperature is relatively low, the mechanism is described more accurately as condensation (absorption) of CO_2 into the oil phase.[9] In CO_2/crude-oil systems that display more than one liquid phase in conjunction with a vapor phase, the mechanism is one of condensation and can account for a phenomenon reported by Shelton and Yarborough,[7] namely that two liquid phases can form either with or without vapor being present. The displacement then has the appearance of a liquid-liquid extraction process. In any case, the miscibility development mechanism is related directly to the phase equilibria of the CO_2/reservoir-fluid system.

All these mechanisms are characterized by high recoveries in the laboratory. Simon *et al.*[6] suggested that IFT effects are responsible for high recoveries in a vaporizing situation and might be equally effective in a liquid-liquid extraction situation; consequently, it is desirable to study tension behavior along with the phase behavior of CO_2/hydrocarbon systems, as we do here. We make use of a molecular theory, the gradient theory of inhomogeneous fluid, which unifies phase and tension behavior in a practicable way. Such an approach has not been followed before.

The CO_2 / propane (C_3) / decane (C_{10}) system was selected for this study because CO_2-C_3 and CO_2-C_{10} binary phase equilibria data for wide ranges of temperature and pressure are available. Propane represents the light ends and decane the heavier components. Of course, CO_2 and reservoir oils do not have exactly the same phase (and therefore tension) behavior as the simple binary and ternary systems discussed here, but as Hutchinson and Braun[8] demonstrated, these systems can give at least a qualitative description of the phase behavior of CO_2/crude-oil systems, although Rathmell *et al.*[10] indicated that when large amounts of CO_2 and methane (C_1) are both present, a quaternary diagram is needed to account for the observed behavior.

Phase Behavior Calculations

The design of a CO_2 flooding process requires accurate phase behavior predictions of the equilibrium between the oil in place and the injected CO_2. In one approach, the experimental data and extrapolations or interpolations are used in the process simulator. This approach can be quite inaccurate unless a great deal of data are available. Alternatively, an EOS can be postulated and its adjustable parameters fit to a limited amount of data. This is clearly the best approach when a good EOS can be found. As shown in the next section, it is the only feasible approach when IFT are to be predicted along with phase behavior.

*Now with the U. of Southern California.

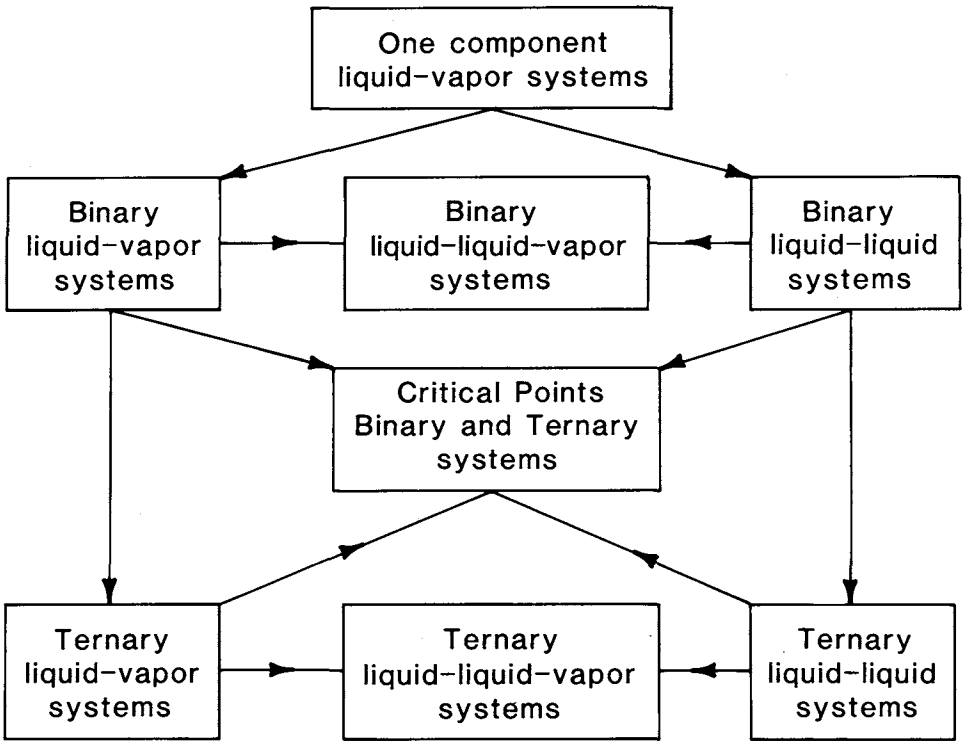

Fig. 1—Flow chart of phase behavior calculations.

For our present purposes, we chose for computations a cubic equation of the van der Waals type, either the Peng and Robinson equation (PREOS)[11] or the Redlich-Kwong-Soave equation (RKSEOS).[12,13]

With an EOS, the existence of multiple phases in equilibrium and their compositions are determined by equating the pressures and chemical potentials in all the phases. Chemical potentials are derived from the EOS.

Traditionally, the phase behavior of systems involving oil, a complicated multicomponent fluid, is shown on (pseudo-) ternary diagrams that include phase splits, the direction of the tie-lines between the equilibrium phases on the diagram, and the location of critical points. To determine the ternary phase diagram our strategy here is to find: (1) the vapor-liquid spinodal and critical point and then a succession of coexisting equilibrium vapor and liquid phase densities in each of the three single-component systems; (2) the vapor-liquid binodal and tie lines in each of the three binary systems, in each case starting at a pressure slightly above the vapor pressure of the less volatile component; (3) the liquid-liquid binodal and tie-lines—if indeed there is a miscibility gap at any pressure-temperature combination in each of the three binary systems—in each case starting from a pressure slightly above the vapor pressure of the more volatile component and from a pair of trial component densities that are very nearly those of pure components; (4) the liquid-liquid-vapor tie line if it exists; (5) the ternary vapor-liquid binodals and tie lines that evolve from each of the three binary vapor-liquid binodals, in each case starting with a small amount of the third component; (6) the ternary liquid-liquid binodals and tie lines that evolve from each of the binary liquid-liquid binodals—here there is but one—in each case starting with a small amount of the third component; (7) the ternary vapor-liquid-liquid tie triangles that evolve from the binary three-phase tie line, starting at a pressure slightly above the three-phase equilibrium pressure of the binary. At every stage in the computation, the spinodals and critical points or loci can be found if needed to locate the tip of the binodal dome. The strategy is summarized in Fig. 1. It is not a general strategy for all kinds of ternary fluid phase equilibria, for it relies on prior knowledge about the nature of the system's phase diagram, but the strategy is applicable to systems with phase behavior similar to that of CO_2/hydrocarbon mixtures. With little prior knowledge of a system's phase diagram, locating the spinodals and critical loci becomes a crucial first step in computing the phase diagram.

For the EOS used in this study, the following dimensionless variables are convenient.

$$\tilde{p}\equiv\frac{pb_1^2}{a_{11}},\ \tilde{n}\equiv nb_1,\ \tilde{n}_j\equiv b_1,\ \tilde{T}\equiv\frac{Tkb_1}{a_{11}},$$

$$\tilde{b}\equiv\frac{b}{b_1},\ \tilde{a}\equiv\frac{a}{a_{11}},\ \tilde{\mu}_j\equiv\mu_j\frac{b_1}{a_{11}},\quad\ldots\ldots\ldots\ldots(1)$$

where

p = pressure,
n = total density,
n_j = density of component j,
T = temperature,
k = Boltzman's constant,
m_j = chemical potential of component j,
a = energy parameter of the EOS, and
b = volume parameter of the EOS.

The parameters a_{11} and b_1 are those of CO_2. Henceforth, the numerical values given are those of dimensionless variables unless the dimensions are given. Details of the strategy are described next.

One-Component Liquid-Vapor Binodal. At a succession of temperatures below critical, the equations of chemical and mechanical equilibrium, $\mu(n_\alpha^V)=\mu(n_\alpha^L)$ and $p(n_\alpha^V)=p(n_\alpha^L)$, were solved by Newtonian iteration. Because typical temperatures of the oil fields considered for CO_2 flooding are below 323.15 K [50°C], all calculations here but one are for the range 273.15 K to 323.15 K [0 to 50°C]. The initial estimates of the liquid and vapor densities, n_α^L and n_α^V, were crucial, for they had to be accurate enough to fall within the domains of convergence of Newton's method. Far below critical, the two nonzero densities that make pressure vanish in the EOS are always good estimates and for the cubic EOS (e.g., Peng-Robinson,[11] Soave,[12] Redlich-Kwong,[13] or van der Waals) are simply found as roots of the quadratic equation obtained by setting $p=0$. For the majority of our computations we used the PREOS. For economy here we report the details only for that equation; however, we compared the PREOS and RKSEOS equations and found their predictions to be quite similar. At 273.15 K [0°C], the $p=0$ estimates led to convergence within four iterations. The convergence criterion was that the sum of the squares of the residuals be less than a small value ϵ (we chose 10^{-20} for pure component calculations). Thereafter, temperature was increased in increments of five to ten degrees and zero-order continuation was used—i.e., the last solution for densities was used as the initial estimate. Four iterations sufficed for convergence. With smaller increments of temperature (e.g., three degrees), two iterations sufficed for convergence. Care was needed in selecting the temperature increment. If it was too large, a trivial solution was sometimes obtained—i.e., equal densities of both phases. The increment required to avoid the trivial solution depends on the EOS. For example, with the van der Waals EOS, a temperature increment greater than two degrees yielded trivial solutions, whereas with the PREOS, the temperature increment could be as large as 20°, although the number of iterations for convergence increased. The convergence rate always approached quadratic, as it should when Newtonian iteration is implemented correctly.

Binary Liquid-Vapor Binodal. There are two degrees of freedom in this case. With the pressure set at p, the equations solved are

$$\mu_i(\boldsymbol{n}^L)=\mu_i(\boldsymbol{n}^V),\ i=1 \text{ and } 2$$

and

$$p(\boldsymbol{n}^L)=p(\boldsymbol{n}^V)=p,$$

where $\boldsymbol{n}$ denotes the set of component densities in phase α. If one mole fraction is set, the chemical potential equations are the same, but the mechanical equilibrium equation becomes $p(\boldsymbol{n}^L)=p(\boldsymbol{n}^V)$, and the fourth equation is

$$y_i^\alpha=\frac{n_i^\alpha}{\sum_{i=1}^{2} n_i^\alpha},$$

where y_i^α is the set mole fraction of component i with density n_i^α in phase α. To complete the specification of a system, temperature is always fixed. It is appropriate to set the pressure slightly above the vapor pressure of the less volatile component, to guarantee that vapor and liquid phases coexist. We take for initial estimates of densities the pure component liquid-vapor equilibrium densities of the less volatile component and set the density of the more volatile component equal to 10^{-2} in the liquid phase. In our experience, the first computation then converged within six iterations. However, in all the liquid-vapor systems studied here or by Carey,[14] it was found that the total density, nb, of liquid phase falls between 0.7 and 0.8. This fact suggested a second method for finding the binodal. Instead of setting pressure, a liquid mole fraction x_i^L is set, and the initial estimate of the liquid density is calculated from

$$n_i^L=\frac{0.75}{\sum_{i=1}^{2} b_i x_i^L},$$

and $n_i^L=x_i^L n^L$. More generally, the value 0.75 in this equation can be replaced with the liquid density of the pure heavy component. For initial estimates of vapor densities, pure component densities can be used. If the mole fraction of the more volatile component in the liquid were set to 0.01, the mixture would be almost pure in the less volatile component, which would guarantee that liquid and vapor phases coexist. With this scheme the first computation converged within five iterations; the convergence criterion was the same as in the single component case (but with $\epsilon \sim 10^{-14}$). The second method—i.e., setting one mole fraction—probably is superior because, with this method, one equilibrium equation is linear in density.

Calculations were started at 273.15 K [0°C]. Newtonian iteration usually was used, the liquid mole fraction of the more volatile component was increased in steps of 0.10, and up to six iterations were needed (four was commonly the number). If the step size was shortened to 0.05, the maximum number of iterations fell to three or four. No adaptive step-size routine was used, and sometimes the chosen step size led to solutions that violate the necessities that all component densities, n_i^α, be positive and the overall density not exceed molecular close-packing—i.e., the condition $\boldsymbol{n}^\alpha b<1$. As an expedient, a relaxation parameter, r^α, was introduced for each phase. If the $(k+1)$ Newton iterate gave positive component densities and $\boldsymbol{n}^\alpha b<1$, the Newton process was continued. If the $(k+1)$ Newton iterate of the density of component i in phase α was negative, r^α was set to 1/10 and provisional component densities were calculated from the relaxation equation

$$n_i^\alpha=(1-r^\alpha)n_i^{\alpha(k)}+r^\alpha n_i^{\alpha(k+1)},$$

where $n_i^{\alpha(k)}$ is the kth Newton iterate. If the sum of the provisional densities did not exceed the limit on phase density that corresponds to molecular close-packing (i.e., $n^{\alpha}b<1$), the provisional densities were adopted as the $(k+1)$ iterate and the Newton process was resumed. Otherwise r^{α} was diminished by a factor of five, and new provisional values were calculated from the relaxation equation and similarly tested. No more than two such search cycles were ever needed to find admissible n_i^{α}.

Once the liquid composition of the more volatile component reached 0.99, the temperature was increased 10 K [10°C] and a new round of calculations carried out in the same way. At temperatures above the critical temperature of the more volatile component and at high liquid mole fractions of this component, first-order continuation, which makes use of the Jacobian of the last Newton iterate, proved cost effective in keeping initial estimates inside the region of convergence within six iterations. Above the critical temperature of CO_2, calculations were stopped at the liquid-vapor critical point.

Binary Liquid-Liquid Binodal. Again there are two degrees of freedom. Temperature and pressure are set; pressure is more appropriate here than in calculating vapor-liquid binodals, because liquid densities are insensitive to pressure. Calculations were started at 273.15 K [0°C]. Since the two bulk phases are quite rich in their respective major component, good initial guesses for each phase were that the density of the rich component is equal to its single component liquid density and that the density of the lean component is 10^{-3}. Calculations were started at a pressure slightly above the vapor pressure of the more volatile component to avoid failure of the iterative calculation. For this starting mixture, the computation converged within six iterations. The convergence criterion was the same as in the liquid-vapor case. No automatic step-size adjuster was available yet; pressure was increased by as much as 810.6 kPa [117.6 psi] with zero-order continuation, and four iterations were enough for convergence. Calculations were continued until the critical pressure of the more volatile component was reached, then temperature was increased 10 K [10°C] and computations resumed. Even near the critical points of liquid-liquid systems there was no need for first-order continuation, because densities are insensitive. Calculations were stopped at 323.15 K [50°C].

Binary Liquid-Liquid-Vapor Tie Line. There is only one degree of freedom, so if temperature is set, the system is completely specified. Calculations were begun at 273.15 K [0°C]. As Orr *et al.*[15] pointed out, the three-phase equilibrium pressure of CO_2/hydrocarbon binaries is bounded above by CO_2 vapor pressure and is close to it. Therefore, for the initial estimates of the three-phase equilibrium densities, binary liquid-liquid and liquid-vapor equilibrium densities at a pressure very close to CO_2 vapor pressure were used. These estimates are excellent; with them only four iterations were needed to meet the convergence criterion. Temperature was increased 10 K [10°C] at a time. Calculations were stopped at the lowest temperature for which there is a liquid-liquid critical point. For some mixtures of CO_2 with alkanes, the three-phase equilibrium disappears before a liquid-liquid critical point appears (e.g., CO_2/hexadecane). In this case, calculation of three-phase equilibrium should be stopped at the temperature at which the binary liquid-vapor equilibrium with a CO_2-rich liquid phase disappears and is replaced by a one-phase region.

Ternary Vapor-Liquid Binodal. There are three degrees of freedom, and the most effective tactic appears to be to set temperature and two liquid mole fractions, because two equilibrium equations (out of six) are linear in liquid densities. Calculations were started at 273.15 K [0°C]. A binary was chosen, and a small amount of the third component (usually the intermediate component) was added to the mixture, so that the mixture was almost a binary one. Binary equilibrium densities were used as the initial estimate of the equilibrium densities. The convergence criterion was the same as for binaries, with $\epsilon \sim 10^{-14}$. The computation of this very first ternary vapor-liquid equilibrium converged within seven iterations. Then temperature and the liquid mole fraction of the most volatile component were held fixed and the liquid mole fraction of the component of intermediate volatility was increased by 0.1 or less, so that each computation converged in not more than six iterations. When the mole fraction step was 0.05, four iterations sufficed with zero-order continuation. When the step was 0.1 but first-order continuation was used, four iterations sufficed. After the liquid mole fraction of the intermediate-volatility component reached 0.90 and the mole fraction of each of the other components was 0.05, the liquid mole fraction of the most volatile component was raised by 0.10, and that of the intermediate volatility component was varied again. Calculations were stopped when the liquid mole fraction of the most volatile component reached 0.90 (so that the other two were 0.05). Then the temperature was increased 5 to 10 K [5 to 10°C] and, with the equilibrium densities at 273.15 K [0°C] as the initial estimate, computations were continued. No difficulty arose because first-order continuation was used when a liquid mole fraction was increased, although when temperature was increased, only zero-order continuation was used. Calculations were stopped at 323.15 K [50°C].

Ternary Liquid-Liquid Binodal. Again there are three degrees of freedom, but now the best tactic is to set temperature, then pressure and one mole fraction in one phase, as discussed above. Calculations were started at 273.15 K [0°C] with a binary liquid-liquid equilibrium to which a very small amount of the third component was added. Pressure was set to the binary equilibrium pressure. Pressure and temperature were held fixed and the composition increased by increments of 0.05 in mole fraction. Newton's method with zero-order continuation converged within four iterations. The mole fraction of the third component was increased until the two liquid phases became miscible—i.e., the plait point was passed. Then pressure was increased 507 kPa [73.5 psi], and the computational cycle was repeated. When the pressure reached a level at which the two-phase equilibrium ceased (i.e., the plait point disappeared) the computation was stopped, the temperature was increased by 10 K [10°C] and then computation was resumed by means of zero-order continuation for the initial estimate. With increasing temperature, the mole fraction of the third component that

miscibilized the two phases fell sharply; the calculations were halted when this mole fraction dropped below 0.01.

Ternary Liquid-Liquid-Vapor Tie Triangle. There are just two degrees of freedom, and temperature and pressure are set because the liquid densities are insensitive to pressure. There are nine simultaneous equations to solve. Setting pressure gives three equations, one for each phase, and the equality of chemical potential gives six equations, two two-phase equilibria for each component. Calculations were started at 273.15 K [0°C] and at the binary three-phase equilibrium pressure. At these conditions the density of the third component in different phases was very small so it was set to 10^{-4} as the first guess. The very first solution required seven iterations. Pressure was increased in steps of 50.7 kPa [7.35 psi] with first-order continuation and with four or five iterations sufficing at each pressure. The computation was stopped when the pressure became high enough to miscibilize the CO_2-rich liquid phase with the vapor phase—i.e., when the critical endpoint was passed. Then temperature was increased 5 K [5°C], and the computational cycle repeated. As temperature rose the pressure range of three-phase ternary equilibria narrowed, so the pressure step needed to be smaller; we fixed it at 41 kPa [5.9 psi] because no routine for adaptively changing parameter stepsize was available then. Finally, the temperature surpassed that at which there is one and only one pressure at which a three-phase ternary equilibrium exists, and the calculation was halted.

Calculations of Critical Points. The method of Heidemann and Khalil[16] (see also Michelsen[17] and Michelsen and Heidemann[18]) begins with locating the spinodal by fixing molar volume and mole fractions (or component densities) and seeking a temperature at which the second variation of free energy vanishes, then fixing temperature and seeking a volume or density at which the third variation of free energy vanishes. Convergence of the alternating one-dimensional (1D) searches is enhanced by clever initial guesses and by premultiplying the expressions for the second and third free energy variations by quantities that smooth the variation of each with respect to temperature or volume. What is involved is actually the calculation of the eigenvector of the free energy Hessian (a matrix of second derivatives of the free energy) that corresponds to the zero eigenvalue. An alternative to this method can be devised using inverse iteration. If w is an estimate of the normalized eigenvector corresponding to the smallest eigenvalue λ_1 of the free energy Hessian J, then the norm of the vector $J^{-1}w$ goes to infinity as λ_1 goes to zero. Thus, in the method used here the inverse of the norm of $J^{-1}w$ is used as the test function in place of Heidemann and Khalil's[16] determinant of the free energy Hessian. Our test function vanishes only at points on the spinodal and eliminates any need for computing the corresponding eigenpair. Once the spinodal is reached, the critical point can be located efficiently by a virtually 1D search along the spinodal by means of the directional derivative of the third variation, the spinodal itself being tracked by varying temperature with densities or volume and mole fractions held fixed. Details of the scheme are available elsewhere.[19]

Critical points in the binary and ternary systems studied here were located with the new scheme, which proved more cost effective than the method of Heidemann and Khalil or that of Michelsen and Heidemann. We suspect that it would be even more advantageous for systems of more than three components.

IFT Calculation

Theoretical and semiempirical predictions of IFT have lagged behind predictions of phase behavior of fluids. In recent years, however, the molecular theory of interfacial phenomena has advanced considerably.[20] Of particular significance for practical computations of gas-liquid surface tensions and liquid-liquid IFT is gradient theory. The inputs of gradient theory are the free energy density, f^0, of homogeneous fluid and the influence parameters, $c_{\alpha\beta}$, of inhomogeneous fluid. The influence parameters have been related rigorously[21,22] to the mean-square range of the direct correlation function of homogeneous fluid. Thus, all of the inputs of the gradient theory of inhomogeneous fluid can be derived from the properties of homogeneous fluid.

Consider a planar interface between two bulk phases at equilibrium, and denote by x the distance normal to the interface. According to gradient theory, the number density $n_\alpha(x)$ of component α at position x in a ν-component, inhomogeneous fluid obeys the equilibrium equation (a condition of minimum free energy):

$$\sum_\beta c_{\alpha\beta}\frac{d^2n_\beta}{dx^2}-\frac{1}{2}\sum_\gamma\sum_\beta\frac{\partial c_{\gamma\beta}}{\partial n_\alpha}\frac{dn_\gamma}{dx}\frac{dn_\beta}{dx}=\frac{\partial\Phi}{\partial n_\alpha}, \quad \ldots\ldots (2)$$

where Φ is a grand thermodynamic potential energy density defined by

$$\Phi(\boldsymbol{n})\equiv f^0(\boldsymbol{n})-\sum_\alpha\mu_\alpha, \quad \ldots\ldots (3)$$

where $\boldsymbol{n}$ denotes the set of densities $n_1 \ldots n_\nu$ and μ_α is the chemical potential of component α. Multiplying Eq. 2 by dn_α/dx, summing over α, and integrating the result yields

$$\sum_\alpha\sum_\beta c_{\alpha\beta}\frac{dn_\alpha}{dx}\frac{dn_\beta}{dx}=2[\Phi(\boldsymbol{n})-\Phi_B]\equiv 2\Delta\Phi(\boldsymbol{n}), \quad \ldots (4)$$

where Φ_B is a constant of integration. The boundary conditions for a planar interface between bulk phases 1 and 2 are $n_\alpha(x=-\infty)=n_\alpha^{(1)}$ and $n_\alpha(x=+\infty)=n_\alpha^{(2)}$ where $\alpha=1\ldots\nu$. These conditions are equivalent to the usual chemical and mechanical equilibrium conditions.

IFT originates in the density and composition nonuniformity within the transition region between the bulk phases. The gradient theory formula for tension is[14]

$$\sigma=\int_{-\infty}^{\infty}\left(\sum_\alpha\sum_\beta c_{\alpha\beta}\frac{dn_\alpha}{dx}\frac{dn_\beta}{dx}\right)dx=2\int_{-\infty}^{\infty}\Delta\Phi(\boldsymbol{n})dx. \quad \ldots\ldots (5)$$

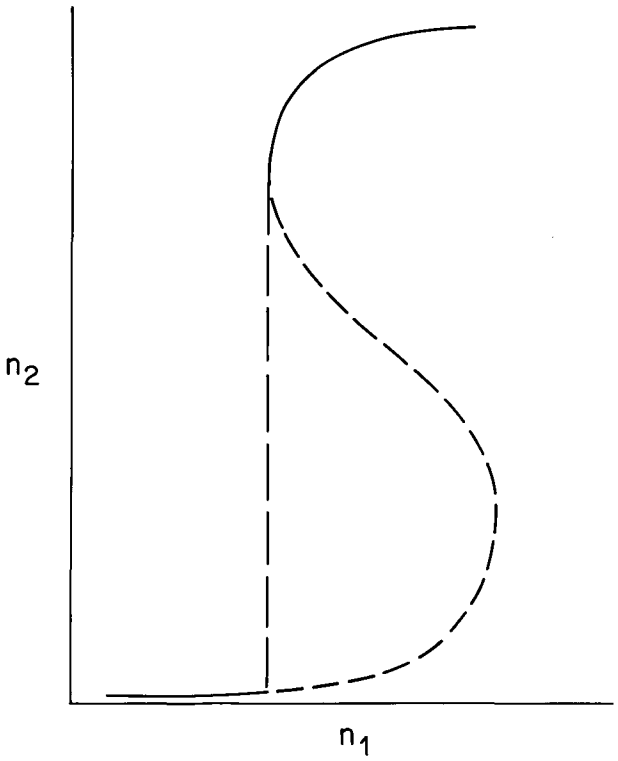

Fig. 2—Double-valued density profile.

One way to find σ is to solve Eq. 2 for the density profile $n_\alpha(x)$ and compute the IFT from Eq. 5. However, from the chain rule of differentiation,

$$\frac{dn_\alpha}{dx}=\frac{dn_\alpha}{dn_1}\frac{dn_1}{dx}, \quad \ldots\ldots\ldots\ldots\ldots\ldots\ldots\ldots (6)$$

$$\frac{d^2n_\alpha}{dx^2}=\left(\frac{dn_1}{dx}\right)^2\frac{d^2n_\alpha}{dn_1^2}+\frac{d^2n_1}{dx^2}\frac{dn_\alpha}{dn_1}, \quad \ldots\ldots\ldots (7)$$

and, from Eq. 4, it follows that

$$\left(\frac{dn_1}{dx}\right)^2=\frac{2\Delta\Phi(\boldsymbol{n})}{\sum_\alpha^\nu\sum_\beta^\nu c_{\alpha\beta}\frac{dn_\alpha}{dn_1}\frac{dn_\beta}{dn_1}}. \quad \ldots\ldots\ldots\ldots (8)$$

This can be used to eliminate the spatial variable and obtain $(\nu-1)$ equations in the independent variable n_1. If $c_{\alpha\beta}$ is assumed independent of composition, an assumption that is supported by the work of McCoy and Davis[23] and the results of Carey *et al.*,[24] the governing equation (Eq. 2) reduces to

$$\sum_\beta c_{\alpha\beta}\frac{d^2n_\beta}{dx^2}=\frac{\partial\Phi}{\partial n_\alpha}. \quad \ldots\ldots\ldots\ldots\ldots\ldots (9)$$

This can be rewritten in matrix form as

$$\frac{d^2\boldsymbol{n}}{dx^2}=\frac{F(\boldsymbol{n})}{|c|}, \quad \ldots\ldots\ldots\ldots\ldots\ldots\ldots (10)$$

where $|c|$ is the determinant of the influence parameter matrix. In combination, Eqs. 6, 7, 8, and 10 give

$$\left(\sum_\alpha^\nu\sum_\beta^\nu c_{\alpha\beta}\frac{dn_\alpha}{dn_1}\frac{dn_\beta}{dn_1}\right)\left(F_1\frac{dn_\gamma}{dn_1}-F_\gamma\right)$$

$$-2\Delta\Phi(\boldsymbol{n})\,|c|\,\frac{d^2n_\gamma}{dn_1^2}=0 \quad \ldots\ldots\ldots\ldots\ldots (11)$$

for $\gamma=2\ldots\nu$, where F_γ is the γth component of F. In this way, the problem with the independent variable x defined in an unbounded domain $(-\infty, +\infty)$ is transformed to a problem with independent variable n_1 defined in the bounded domain $[n_1^{(1)}, n_1^{(2)}]$. Of course, n_1 must be a monotonic function of x; if it is not a monotonic function over the entire domain, then the individual equations in Eq. 11 are solved over that part of the domain in which n_1 is a monotonic function of x, and over the rest of the domain the independent variable n_1 is changed to another component density, say n_2, which is a monotonic function of x. The procedure is repeated in case n_2 also is not monotonic. In any event, the surface tension or the IFT is given by

$$\sigma=\sum_i\int_{n_i}^{n_i+\Delta n_i}\sqrt{2\Delta\Phi(\boldsymbol{n})\sum_\alpha\sum_\beta c_{\alpha\beta}\frac{dn_\alpha}{dn_i}\frac{dn_\beta}{dn_i}}\,dn_i, \quad \ldots\ldots\ldots\ldots\ldots\ldots (12)$$

where i denotes the component for which Δn_i is the range over which n_i is monotonic and, therefore, is the independent variable.

In most cases, more than one component density was required as an independent variable to span the interface. The relationship between the pure component influence parameters, $c_{\alpha\alpha}$, and the cross term, $c_{\alpha\beta}$, is not yet settled. Because these terms represent weighted energy parameters, $c_{\alpha\beta}$ was scaled in the same manner as the bulk energy parameter $a_{\alpha\beta}$ of the equation of state:

$$c_{\alpha\beta}=(1-\delta^c_{\alpha\beta})\sqrt{c_{\alpha\alpha}c_{\beta\beta}}, \quad \ldots\ldots\ldots\ldots\ldots (13)$$

where $\delta^c_{\alpha\beta}$ is a mixing parameter. Stability requires that $\delta^c_{\alpha\beta}$ lie between zero and one.[14] The geometric mixing rule ($\delta^c_{\alpha\beta}=0$) carries with it a special bonus, namely that the profile equations, Eq. 11, are reduced to the algebraic equations[14]

$$\sqrt{c_{\alpha\alpha}}\,\Delta\mu_1(\boldsymbol{n})=\sqrt{c_{11}}\,\Delta\mu_\alpha(\boldsymbol{n}), \quad \ldots\ldots\ldots\ldots (14)$$

where $\Delta\mu_\alpha=\mu^o_\alpha(\boldsymbol{n})-\mu_\alpha$, $\mu^o_\alpha(\boldsymbol{n})$ is the chemical potential of component α, and α equals $2\ldots\nu$. The prediction of surface tension of binary and ternary normal alkane mixtures with the geometric mixing rule is quite good.[14,24]

To calculate surface tension between two phases, the interfacial composition profile first must be determined. If the influence parameters obey the ideal (geometric) mixing rule $\delta^c_{\alpha\beta}=0$, then the algebraic equations, Eq. 14, have to be solved. These algebraic equations fix the densities of all but one component, a component that must be chosen carefully. Fig. 2 provides an example: passing from Bulk Phase A to Bulk Phase B by advancing n_1 would never locate the dashed part of the curve, and a corresponding locus of points would be missed by starting from Bulk Phase B. To avoid the problem in binary systems, it suffices to compute

$$\frac{dn_2}{dn_1}=\frac{\sqrt{c_{11}}\frac{\partial\mu_2}{\partial n_1}-\sqrt{c_{22}}\frac{\partial\mu_1}{\partial n_1}}{\sqrt{c_{22}}\frac{\partial\mu_1}{\partial n_2}-\sqrt{c_{11}}\frac{\partial\mu_2}{\partial n_1}}, \quad \ldots\ldots\ldots\ldots (15)$$

then set a value of n_2, and compute n_1 from the algebraic equation if $|\,dn_2/dn_1\,|>1$. If $|\,dn_2/dn_1\,|<1$, then n_1 is set and n_2 is computed. In either case an algebraic equation, Eq. 14, is solved by Newton's method. The step size we chose is

$$\Delta n=\sqrt{\sum_{i=1}^{2}\frac{[n_i^{(1)}-n_i^{(2)}]^2}{400}}, \quad \ldots\ldots\ldots\ldots\ldots (16)$$

and the sign of the step is set according to whether the independent density is increasing or decreasing in the interval of computation. This proved small enough that the method converged in two or three iterations after each step. At each step, our initial estimate of the dependent density was always

$$n_i(n_\alpha+\Delta n_\alpha)=n_i(n_\alpha)+\Delta n_\alpha\frac{dn_i}{dn_\alpha}(n_\alpha), \quad \ldots\ldots\ldots (17)$$

where α denotes the independent density and $\Delta n_\alpha=\pm\Delta n$ is the increment by which n_α is advanced. The convergence criterion we used was $|F|<10^{-8}$, where

$$F\equiv\sqrt{c_{22}}\,\Delta\mu_1-\sqrt{c_{11}}\,\Delta\mu_2. \quad \ldots\ldots\ldots\ldots\ldots (18)$$

Finding the interfacial composition profile in a ternary system with $\delta^c_{\alpha\beta}=0$ requires solving not one but two such equations:

$$F_1\equiv\sqrt{c_{22}}\,\Delta\mu_1(\boldsymbol{n})-\sqrt{c_{11}}\,\Delta\mu_2(\boldsymbol{n})=0 \quad \ldots\ldots\ldots (19)$$

and

$$F_2\equiv\sqrt{c_{33}}\,\Delta\mu_1(\boldsymbol{n})-\sqrt{c_{11}}\,\Delta\mu_3(\boldsymbol{n})=0. \quad \ldots\ldots\ldots (20)$$

Again $\boldsymbol{n}=(n_1,n_2,n_3)$ and the boundary (bulk) sets $n^{(1)}$ and $n^{(2)}$ are computed as described earlier. The procedure now is to compute dn_2/dn_1 and dn_3/dn_1 and compare the quantities $|\,dn_i/ds\,|$ where

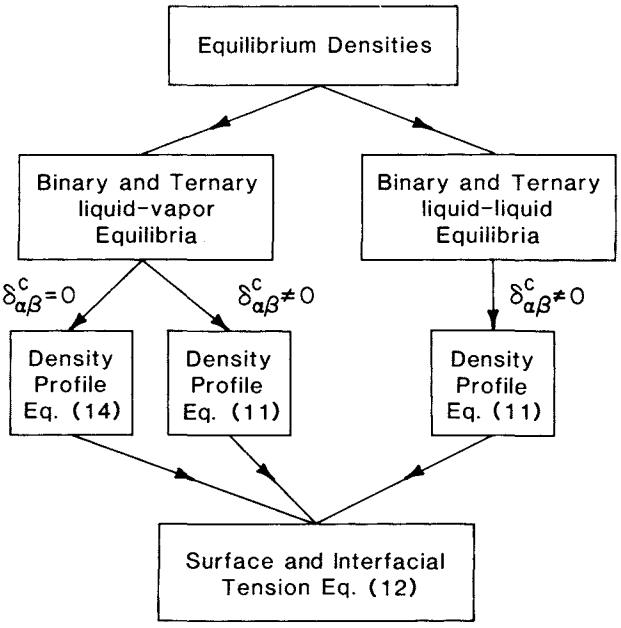

Fig. 3—Flow chart of IFT calculations.

$$ds\equiv\sqrt{\sum_{i=1}^{3}(dn_i)^2} \quad \ldots\ldots\ldots\ldots\ldots\ldots (21)$$

to select, as the new independent variable for incremental advancement, that n_j for which dn_j/ds is the greatest in magnitude (this amounts to what is sometimes called arc-length continuation). This avoids problems associated with multivaluedness of some densities along the phase path; the density increments of all components other than j are virtually certain to be less than Δn_j. At each step, the independent variable is chosen and advanced by Δn_j, and the initial guesses of the other densities were computed from

$$n_i(n_j+\Delta n_j)=n_i(n_j)+\Delta n_j\frac{dn_i}{dn_j}(n_j). \quad \ldots\ldots\ldots (22)$$

Then, Eqs. 19 and 20 were solved by Newton's method, which for each pair of densities converged within four or five iterations because the step size was small. The convergence criterion was $F_1^2+F_2^2<10^{-14}$.

When the mixing parameters do not vanish (i.e., $\delta^c_{\alpha\beta}\neq0$) the differential equations, Eq. 11, must be solved for the $\nu-1$ dependent components of a ν-component system. We solved them by finite differencing to arrive at discretized analogs.

We found that finite differencing with 100 grid points yielded practically the same tension as 500 points, so we used the smaller number. Once the interfacial composition profile was in hand, surface tension was computed from Eq. 12. Up to four iterations for liquid-liquid equilibrium tension and five or six iterations for liquid-

TABLE 1—CRITICAL PROPERTIES AND THE PENG-ROBINSON PARAMETERS FOR THE THREE COMPONENTS[53]

	T_c (K)	p_c (KPa)	ω_a	$a(T_c)$ $\left(\frac{J \cdot m^3}{molecule^2}\right)$	b $\left(\frac{m^3}{molecule}\right)$
CO_2	304.26	30829.9	0.225	1.1×10^{-48}	4.424×10^{-29}
Propane	369.8	37470.9	0.152	2.81×10^{-48}	9.356×10^{-29}
Decane	617.6	62579.8	0.49	1.58×10^{-47}	3.154×10^{-28}

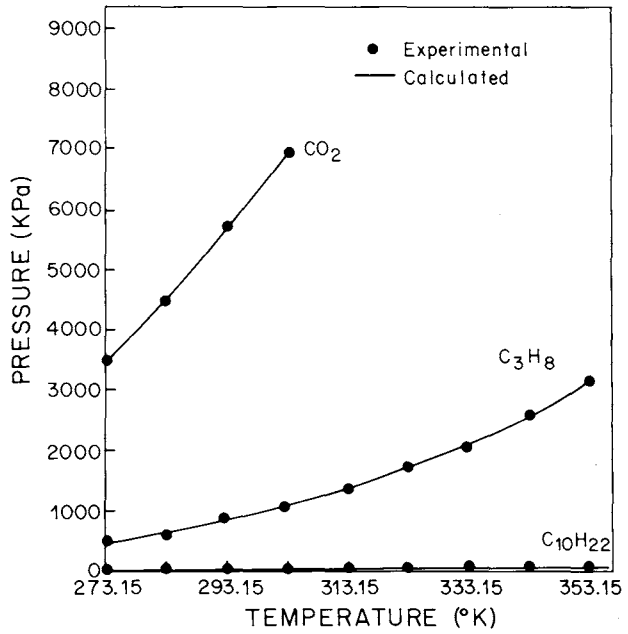

Fig. 4—Vapor pressure of pure components. (Solid curves are calculated from the PREOS.)

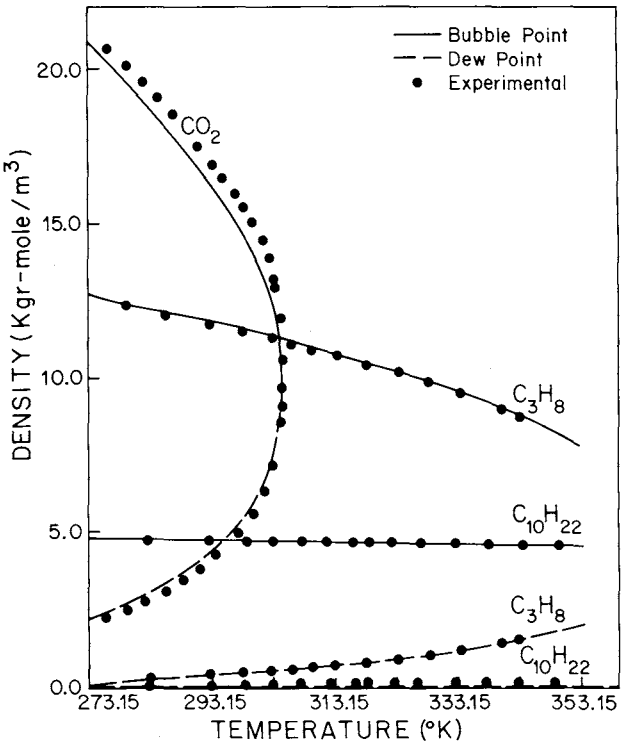

Fig. 5—Liquid-vapor coexistence densities of pure components.

vapor equilibrium tension were required by Newton's method to converge; the convergence criterion was

$$\sum_{i=1}^{100} F_i^2 < 10^{-14}, \quad \ldots\ldots\ldots\ldots\ldots\ldots\ldots (23)$$

where F_i is the residual of Eq. 11 at the ith value of the independent density. Fig. 3 summarizes the steps of our calculations of density profile, surface tension, and IFT.

EOS Models

For the simulation of phase and tension behavior of CO_2/hydrocarbon systems, an EOS must be capable of predicting phase equilibria over a wide range of CO_2 concentrations. Widespread experience to date makes it highly unlikely that any simple EOS can represent equilibrium phase behavior of diverse fluid systems accurately, particularly in regard to component densities in liquid states. Nevertheless, the equations cubic in molar volume (namely that of Redlich and Kwong[13] and its variations by Soave[12] and Peng-Robinson[11]—all descended from van der Waals) are relatively simple and simultaneously accurate enough to be useful for many practical purposes, particularly at low enough temperatures that they predict both liquid- and vapor-range molar volumes well. Other EOS, such as that of Benedict, Webb, and Rubin,[25] are complicated and involve more adjustable parameters than we wished to deal with; and UNIFAC and UNIQUAC[26] were not suitable for this study because an entire EOS was needed for predicting IFT.

Most of the calculations presented here rely on the PREOS[11] to predict phase and tension behavior of binary and ternary CO_2/alkane systems. The PREOS for the pressure $p^0(n)$ of a homogeneous fluid is

$$p^0(n) = \frac{nkT}{1-nb} - \frac{n^2 a(T)}{1+2nb-(nb)^2}, \quad \ldots\ldots\ldots\ldots (24)$$

where a is the energy parameter and b is the volume parameter.

For comparison, we also used the Soave EOS for a few systems. It is given by

$$p^0(n) = \frac{nkT}{1-nb} - \frac{n^2 a(T)}{1+nb}. \quad \ldots\ldots\ldots\ldots\ldots (25)$$

As with any EOS that is applied to multicomponent system, the mixing rules that relate the mixture parameters to those of pure fluids must be hypothesized or else determined from experimental data. We follow the usual practice and hypothesize that

$$b_m=\sum_\alpha y_\alpha b_\alpha,\ a_m=\sum_\alpha\sum_\beta y_\alpha y_\beta a_{\alpha\beta},$$

$$a_{\alpha\beta}=(1-\delta^a_{\alpha\beta})\sqrt{a_{\alpha\alpha}a_{\beta\beta}}, \quad \ldots\ldots\ldots\ldots (26)$$

where

y_α = mole fraction of species α,
$\delta^a_{\alpha\beta}$ = adjustable parameter representing binary interactions (as at Eq. 13),
$a_{\alpha\alpha}$ = pure component energy parameter, and
b_α = pure component volume parameter.

In the PREOS, $a_{\alpha\alpha}$ and b_α are given, as is well known, by[11]

$$b_\alpha=0.0778k\frac{T_{c_\alpha}}{P_{c_\alpha}},\ a_{\alpha\alpha}=a_{\alpha\alpha}(T_{c_\alpha})\beta(T_{R_\alpha},\omega_a)$$

$$\ldots\ldots\ldots\ldots\ldots\ldots\ldots\ldots (27)$$

where

$$a_{\alpha\alpha}(T_{c_\alpha})=0.45724\frac{k^2T^2_{c_\alpha}}{p_{c_\alpha}}, \quad \ldots\ldots\ldots\ldots (28a)$$

$$\beta(T_{R_\alpha},\omega_a)=[1+H(1-T_{R_\alpha}{}^{1/2})]^2, \quad \ldots\ldots\ldots (28b)$$

and

$$H=0.37464+1.54226\omega_a-0.26992\omega_a^2,\ T_{R_\alpha}=T/T_{c_\alpha}.$$

$$\ldots\ldots\ldots\ldots\ldots\ldots\ldots\ldots (29)$$

In the RKSEOS equation, the parameters are given by

$$b_\alpha=0.08664\frac{kT_{c_\alpha}}{p_{c_\alpha}},\ a_{\alpha\alpha}=a_{\alpha\alpha}(T_{c_\alpha})\beta(T_{R_\alpha},\omega_a),$$

$$\ldots\ldots\ldots\ldots\ldots\ldots\ldots\ldots (30)$$

$$a_{\alpha\alpha}(T_{c_\alpha})=0.42747\frac{k^2T^2_{c_\alpha}}{p_{c_\alpha}},\ \beta(T_{c_\alpha},\omega_a)$$

$$=[1+H(1-T_{R_\alpha}{}^{1/2})]^2, \quad \ldots\ldots\ldots\ldots (31)$$

and

$$H=0.480+1.574\omega_a-0.176\omega_a^2. \quad \ldots\ldots\ldots\ldots (32)$$

In these expressions, T_{c_α} and p_{c_α} represent the critical temperature and pressure, respectively, of component α, and ω_a denotes the acentric factor of the αth species. We use the fitted values of $\delta^a_{\alpha\beta}$ reported by Doring and Knapp,[27] which for the PREOS and the RKSEOS are

	CO_2-C_3	CO_2-C_{10}	C_3-C_{10}
PREOS	0.124	0.113	0
RKSEOS	0.128	0.129	0

Table 1 presents the critical properties of CO_2, C_3, and C_{10} and the values of $a_{\alpha\alpha}$ and b_α.

Phase Behavior of CO_2-C_3-C_{10} Mixtures

C_3 represents the light hydrocarbons and C_{10} the heavier ones in crude oil. When a more realistic model than this pseudobinary approximation is required, more components can be included without special difficulty in computations of phase and tension behavior, as described above. What follows are patterns of phase behavior predicted with the PREOS for binary and ternary mixtures of C_3, C_{10}, and CO_2. These results indicate how the PREOS performs and where miscible and low-tension regions fall in the phase diagram.

One-Component Systems. The PREOS and RKSEOS best predict the saturated vapor pressure. This point is illustrated in Fig. 4 by the agreement between measurements and PREOS predictions for CO_2, C_3, and C_{10}. Fig. 5 illustrates the poorer agreement in the case of liquid-vapor coexisting densities for CO_2; the predictions for C_3 and C_{10} are satisfactory. In fact, none of the cubic equations does well at predicting coexisting densities.[28,29]

Two-Component Systems. Binary mixtures of CO_2 with normal alkanes from C_1 through heptane (C_7) have only liquid-vapor miscibility gaps and no liquid-liquid ones above 273.15 K [0°C].[30] Pressure-composition diagrams predicted by the PREOS for CO_2 and C_3 at three temperatures that span the range of interest appear in Fig. 6. They agree quite well with the data, an impression that is substantiated by error analysis summarized later in Fig. 9. Experimental data for this system have been reported by Reamer *et al.*[31] and Poettmann and Katz.[32] At 323 K [49.85°C], the CO_2/C_3 mixture has an upper critical pressure of 6400 kPa [928.2 psi], with a CO_2 mole fraction of 0.63. Also, at this temperature there is an interesting progression of liquid-vapor compositions as pressure increases from the minimum dewpoint pressure (1350 kPa [195.8 psi]). At this minimum, the mole fractions of each component in liquid and vapor are, of course, the same. Raising pressure to about 1650 kPa [239.3 psi] enriches the vapor phase in CO_2 but impoverishes the liquid phase, until at 1650 kPa [239.3 psi] the liquid phase is almost a pure component. But further pressure increase enriches both phases in CO_2. Thus, the pressure-cycle separation of CO_2 and C_3 would be especially effective at 323 K [49.85°C] if such predicted behavior is real.

In binary mixtures of CO_2 and the normal hydrocarbons heavier than C_7, coexisting liquid-vapor, liquid-liquid, and liquid-liquid-vapor phase splits have been observed above 273.15 K [0°C].[30] The patterns exhibited by CO_2 with normal hydrocarbons ranging from octane (C_8) to tridecane (C_{13}) are illustrated by Fig. 7.

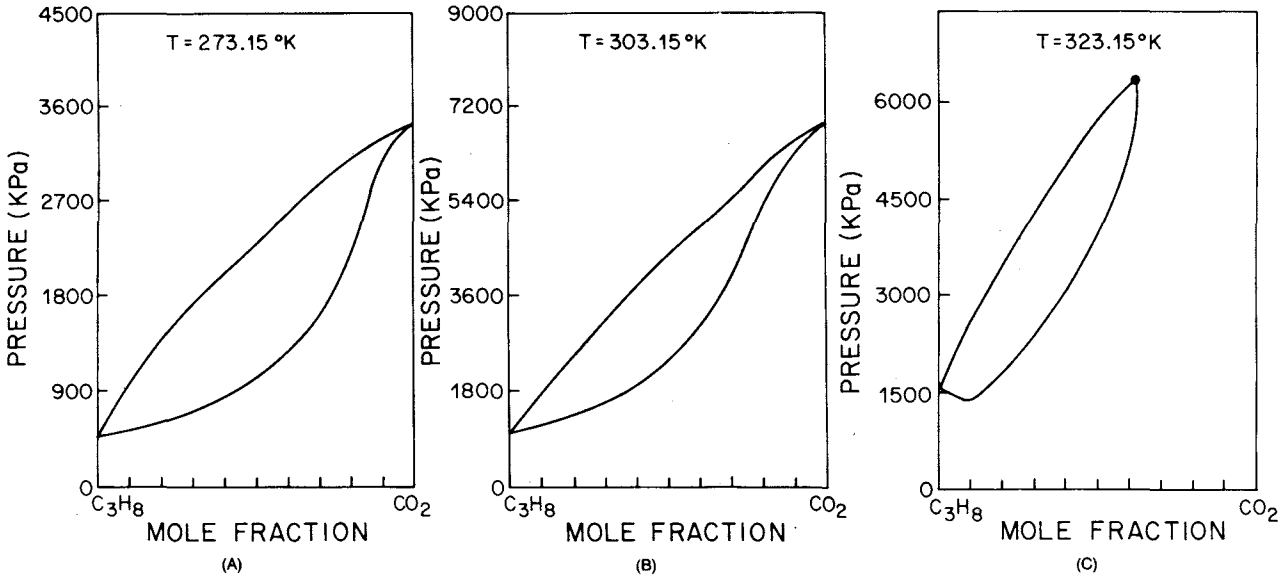

Fig. 6—Phase diagrams for CO_2-propane mixtures at different temperatures.

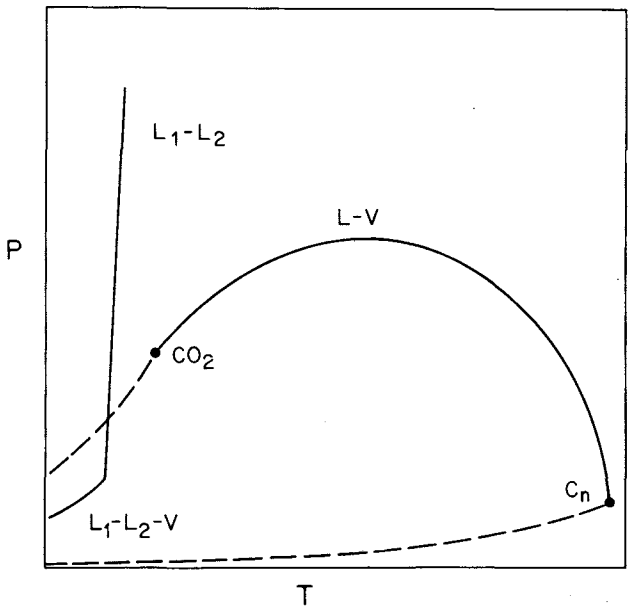

Fig. 7—Qualitative pressure-temperature diagram for CO_2-C_n ($8 \le n \le 13$) mixtures.

Pressure-composition diagrams predicted by the PREOS for CO_2-C_{10} mixtures at three different temperatures are shown in Fig. 8. The patterns of phase splits agree with those that have been observed. Liquid-vapor compositions and the temperatures of phase splits have been measured,[33-38] but liquid-liquid compositions have not been studied. At 273.15 K [0°C], binary mixtures of CO_2 and C_{10} at low pressures separate into a liquid and a vapor phase. As pressure is increased, a value is reached at which coexisting C_{10}-rich liquid (L_2), CO_2-rich liquid (L_1), and CO_2-rich vapor (V) phases (Fig. 8A) form. In the pressure range from the three-phase coexistence pressure up to the vapor pressure of pure CO_2, either L_1-L_2, L_1-V or single-phase mixtures appear, depending on the composition. Above the vapor pressure of CO_2, only coexisting L_1-L_2 or one-phase regions are predicted. With increasing temperature (Fig. 8B) the two liquid phases at the L_1-L_2-V coexistence pressure become increasingly similar, and the L_1-L_2 region separates from the L_2-V region (Fig. 8C). An upper critical point (with respect to pressure) appears on the L_2-V coexistence curve. The pressure of the L_1-L_2 lower critical point rises sharply with increasing temperature. The temperature of separation of the L_2-V and L_1-L_2 coexistence curves has been observed for CO_2 and C_{10} to be about 248.15 K [−25°C]. The value predicted by the PREOS is 318.15 K [45°C]. The discrepancy with experiment could be reduced by letting the interaction parameters, $\delta^a_{\alpha\beta}$, vary with temperature, though at the price of more data to fit $\delta^a_{\alpha\beta}$ and, therefore, a less predictive theory.

In Fig. 9, the mean deviations (as percentages of experimental value) of the Peng-Robinson predictions of liquid-vapor equilibria compositions (mole fractions) from the data of Reamer and Sage[35] are presented; the mean is simply the arithmetic average of individual deviations. At each temperature liquid-vapor equilibrium compositions were calculated at the same pressures as Reamer and Sage's measurements. Complete details are given in Ref. 19. As can be seen, the errors are less than 11%, the worst being at 277.59 K [4.44°C] and the discrepancy falling sharply as temperature increases. For comparison, liquid-vapor predictions were made for the same conditions with the RKSEOS. The errors summarized in Fig. 10 demonstrate that there is little reason to choose between the PREOS and RKSEOS.

Experiments indicate that the L_1-L_2-V coexistence pressure of mixtures of CO_2 and normal alkanes is bounded from above by the vapor pressure of pure CO_2.[15] In fact, the coexistence pressure is close to the CO_2 vapor pressure. This behavior is predicted by the PREOS (Fig. 11). As was pointed out in connection with

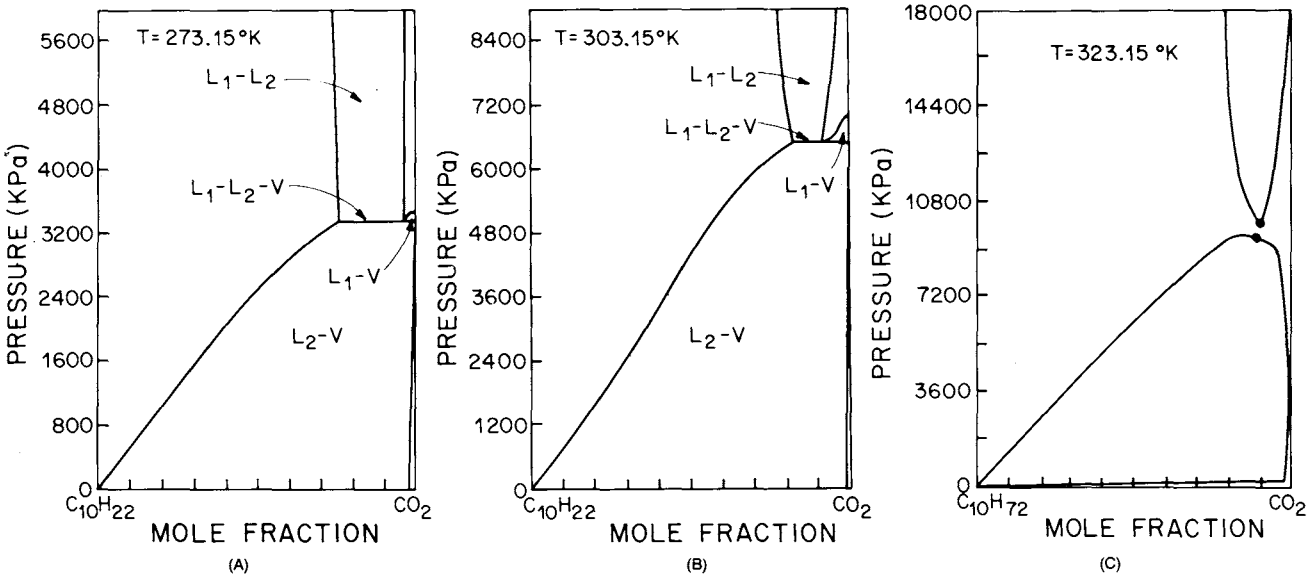

Fig. 8—Phase diagrams for CO_2-decane mixtures at different temperatures.

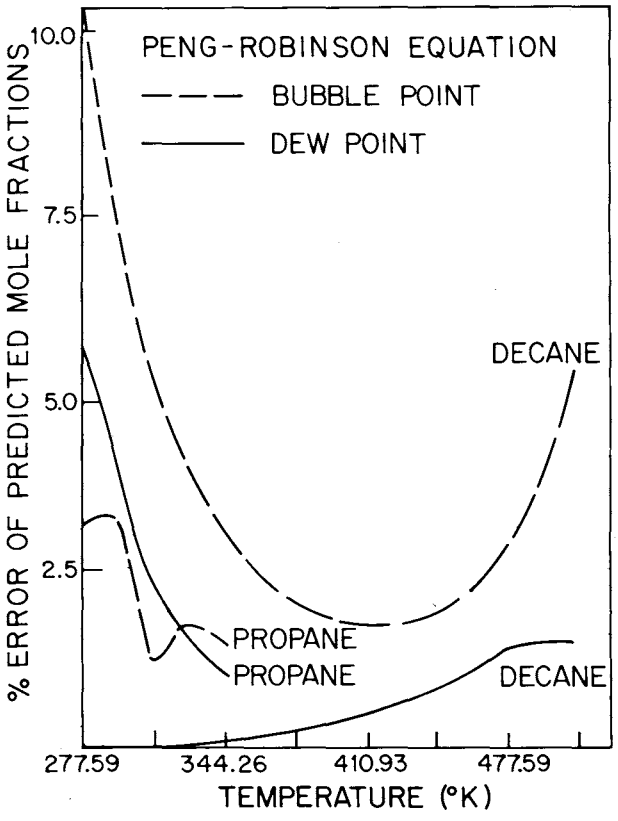

Fig. 9—Comparison of PREOS and experiment—percent error of mole fractions in coexisting liquid and vapor phases.

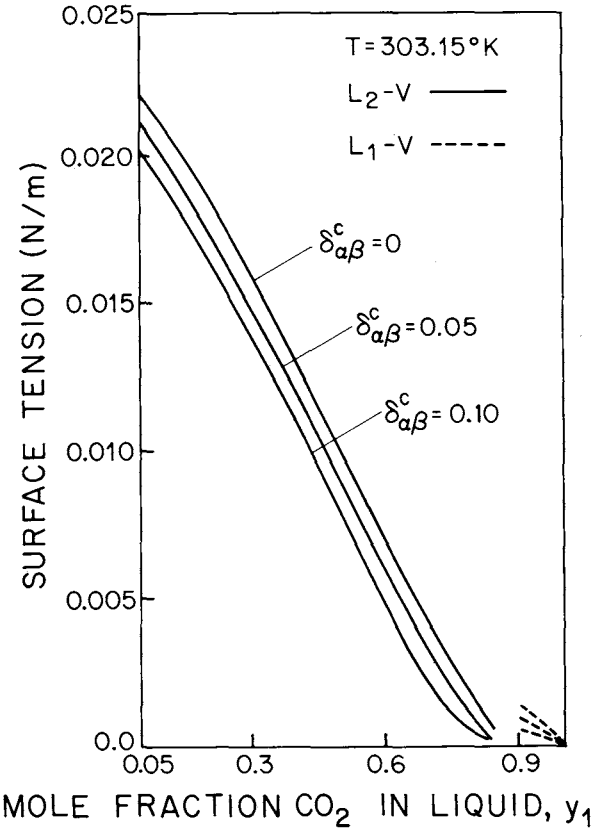

Fig. 10—Comparison of RKSEOS and experiment—percent error of mole fractions in coexisting liquid and vapor phases.

phase behavior calculations, the proximity of the two pressures is useful in getting an initial estimate of the equilibrium densities of the three phases.

Why two liquid phases separate in CO_2 mixtures with the heavier hydrocarbons but not in those with the lighter ones is an interesting question that can be resolved by examining the trends in the parameters of the PREOS. In dimensionless form, the parameters are $\tilde{a}_{22}=a_{22}/a_{11}$, $\tilde{b}_2=b_2/b_1$, and δ'_{12}, where CO_2 is Component 1 and the hydrocarbon is Component 2. The energy parameter, a_{22}, and the size parameter, b_2, of C_1 are almost equal to those of CO_2—i.e., $\tilde{a}_{22}\approx 1$ and $\tilde{b}_2\approx 1$. So the mixture is almost ideal, and there is no tendency of molecules to segregate. As the hydrocarbon increases in molecular

TABLE 2—COMPARISON OF THE PENG-ROBINSON PREDICTION OF L_1-L_2-V EQUILIBRIA FOR CO_2-DECANE MIXTURES WITH THE EXPERIMENTAL DATA OF KULKARNI *et al.*

Temperature (K)	Pressure Experimental (kPa)	Pressure Predicted (kPa)	CO_2 Mole Fraction Experimental		CO_2 Mole Fraction Predicted	
			L_1	L_2	L_1	L_2
235.65	1057.9	1082.2	0.974	0.577	0.9964	0.541
236.15	1074.1	1101.4	0.973	0.582	0.9963	0.545
238.15	1151.1	1181.5	0.970	0.602	0.9957	0.556
240.15	1233.15	1266.6	0.965	0.627	0.9951	0.568
242.15	1381.3	1355.8	0.96	0.659	0.9944	0.579
244.15	1413.52	1449.0	0.954	0.695	0.9936	0.590
246.15	1508.8	1546.25	0.942	0.734	0.9927	0.602
248.15	1610.1	1649.6	0.916	0.783	0.9916	0.613

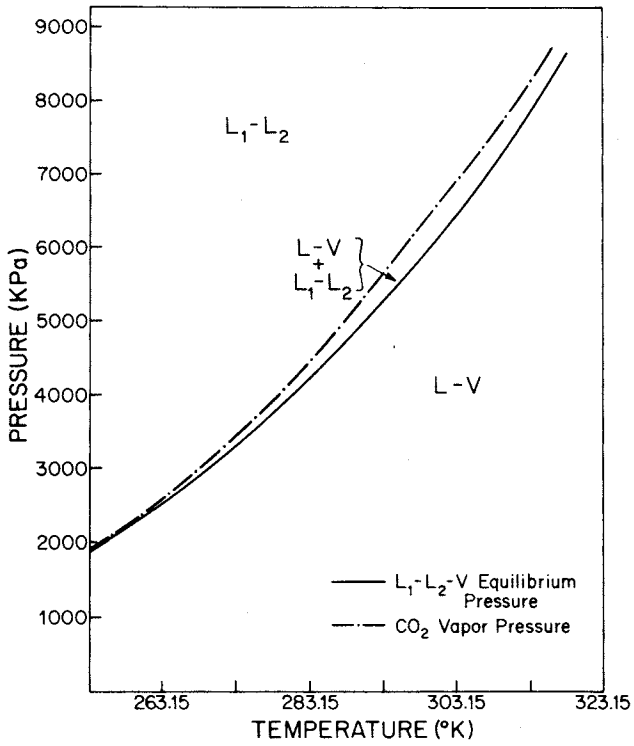

Fig. 11—Multiple-phase regions for CO_2-decane mixtures.

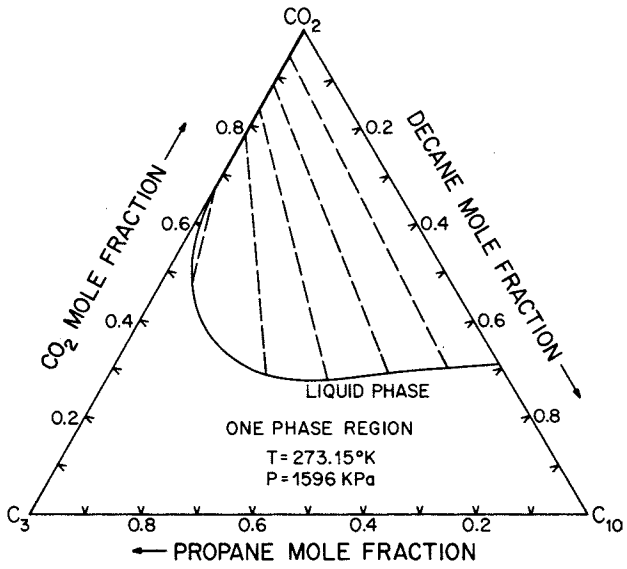

Fig. 12—Phase behavior of CO_2-propane-decane at 1596 kPa [231.4 psi] and 273.15 K [0°C].

weight, both the energy and size parameters increase. Mismatched energy parameters (i.e., $\tilde{a}_{22}$ far from unity) favor molecular segregation and thereby oppose the entropic tendency to mix thoroughly. At some characteristic value of $\tilde{a}_{22}$, the segregation tendency prevails and the liquid splits into two liquid phases. It appears that this transition occurs at about C_8 in the alkane series.

Table 2 compares the predictions of the PREOS of L_1-L_2-V equilibria in CO_2-C_{10} mixtures with the data of Kulkarni *et al.*[38] The predicted equilibrium pressures match the experiments well, the differences nowhere exceeding 46 kPa [6.7 psi], but the predicted equilibrium compositions are not good.

Three-Component Systems. The special advantage of EOS models such as the PREOS and RKSEOS comes in the predictions of the phase behavior of multicomponent mixtures because all the parameters are fitted to one-component and two-component data and phase behavior of a mixture of any number of these components can be predicted. In this section, we illustrate the use of the PREOS by predicting the phase behavior of CO_2, C_3, and C_{10}. Although some studies[33,37,39-42] have been made of CO_2 with two normal hydrocarbons, none has been made of this particular ternary mixture. An idea of the reliability of the predictions is provided by the results for one-component and two-component systems discussed above.

Figs. 12 through 14 are the ternary phase diagrams predicted by the PREOS for a temperature of 273.15 K [0°C] and three different pressures. At 3203 kPa [464.6 psi] (Fig. 13), there are three two-phase regions (L_1-V, L_2-V, and L_1-L_2) and a three-phase region (L_1-L_2-V) in the CO_2-rich part of the ternary diagram. The multiple regions arise out of miscibility gaps along both the CO_2-C_3 and CO_2-C_{10} edges of the diagram. At a lower pressure, 1596 kPa [231.5 psi] (Fig. 12), the three-phase region disappears, leaving a liquid-vapor region that grows out of the CO_2-C_{10} liquid-vapor miscibility gap and has a critical point (plait point) near the CO_2-C_3 edge of the diagram. CO_2 and C_3 are miscible in all proportions at this pressure and temperature. As the pressure increases, the CO_2-rich liquid phase becomes closer in

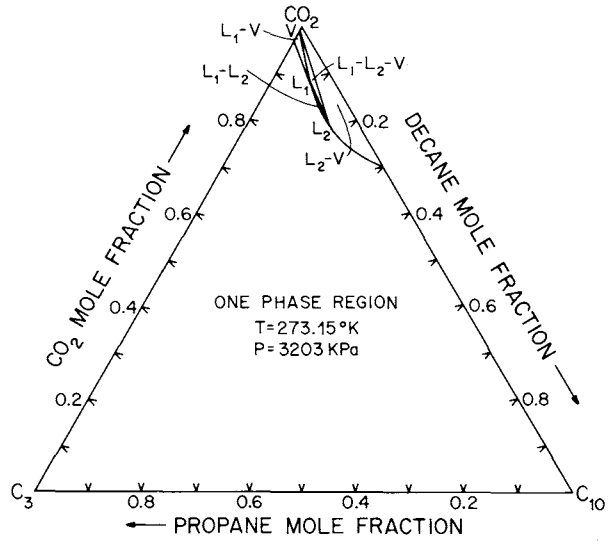

Fig. 13—Phase behavior of CO_2-propane-decane at 3203 kPa [464.6 psi] and 273.15 K [0°C].

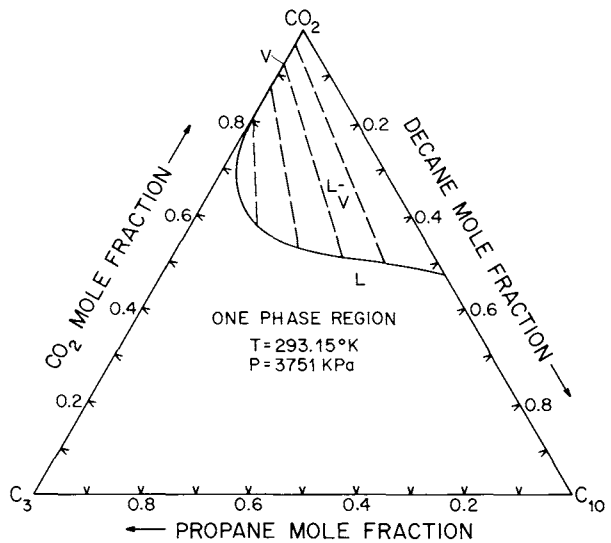

Fig. 15—Phase behavior of CO_2-propane-decane at 3751 kPa [544.0 psi] and 293.15 K [20°C].

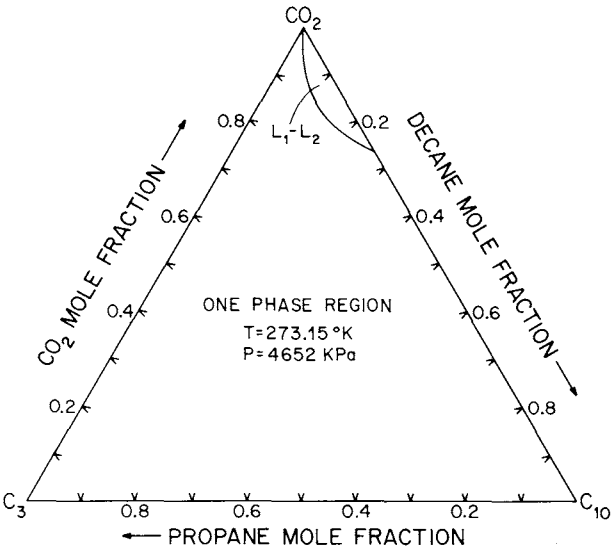

Fig. 14—Phase behavior of CO_2-propane-decane at 4652 kPa [674.7 psi] and 273.15 K [0°C].

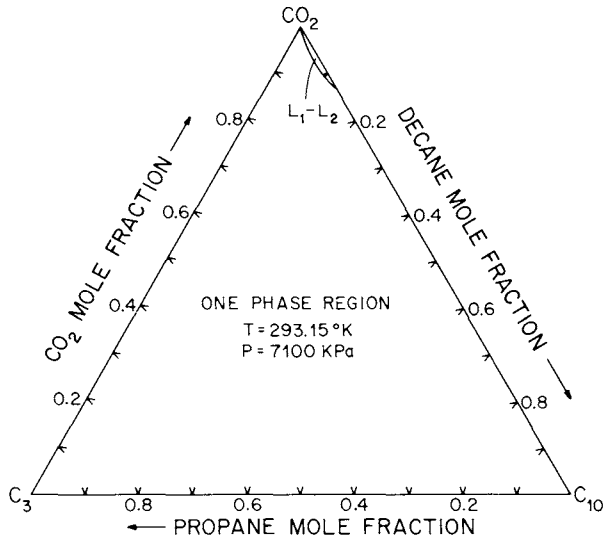

Fig. 16—Phase behavior of CO_2-propane-decane at 7100 kPa [1030 psi] and 293.15 K [20°C].

composition and density to the vapor phase; eventually these two phases coincide (i.e., a critical point is reached) at some CO_2 mole fraction (about 0.45), and only a liquid-liquid region is left. This region arises from the liquid-liquid miscibility gap on the CO_2-C_{10} edge of the ternary diagram. The qualitative features of Figs. 12 through 14 have been observed in mixtures of CO_2 and with light and heavy hydrocarbons and crude oil. If, however, C_3 is replaced by C_1, the resulting sequence is qualitatively different.[15,30]

As the temperature increases, the three-phase region L_1-L_2-V and the two-phase region L_1-L_2 shrink, with the three-phase region disappearing at about 292 K [18.85°C] and the liquid-liquid separation persisting only at very high pressures with very small amounts of C_3. Figs. 15 and 16 show phase behavior of CO_2-C_3-C_{10} mixtures at 293.15 K [20°C]. At this temperature, as pressure rises the binodal goes from a liquid-vapor to a liquid-liquid. Fig. 17 illustrates the multiple-phase regions in CO_2-C_3-C_{10} mixtures as predicted by the PREOS. That many of the patterns can be anticipated from the binary phase behavior is an interesting and potentially useful aspect of the ternary phase behavior.

Tension Behavior of CO_2-C_3-C_{10} Mixtures

Although Rosman and Zana[43] have reported measurements of liquid-vapor surface tension of CO_2/crude-oil mixtures, no tension data are available for CO_2-C_3 or CO_2-C_{10} mixtures. There are very limited data for CO_2-C_4 mixture.[44] Consequently, we cannot determine empirically the values of the mixing parameters. Carey *et al.*[24,25] found that $\delta^c_{\alpha\beta}=0$ provides an excellent approximation for normal alkane mixtures and that the two

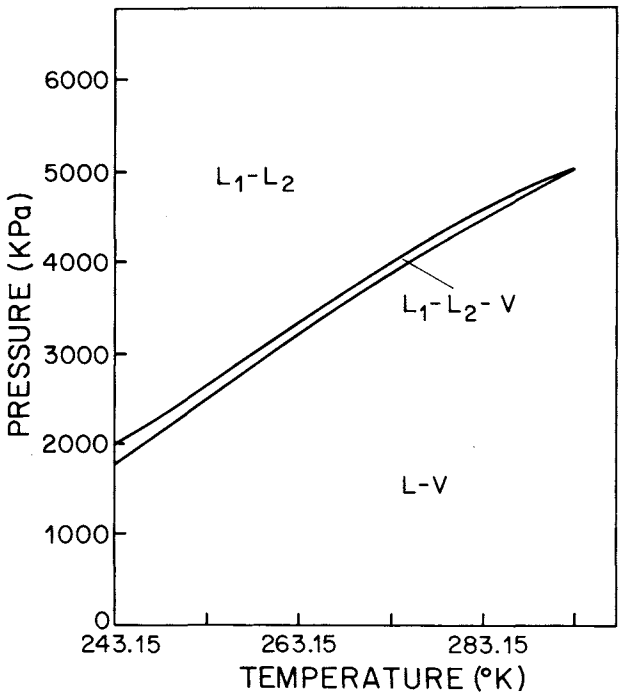

Fig. 17—Multiple-phase regions for CO_2-propane-decane mixtures.

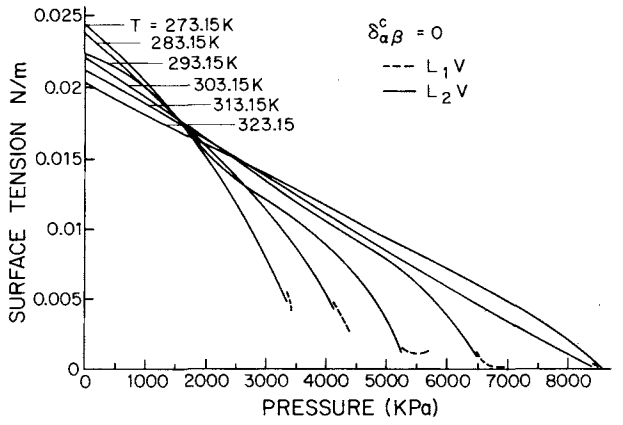

Fig. 18—Liquid-vapor surface tension-pressure isotherms for CO_2-decane mixtures.

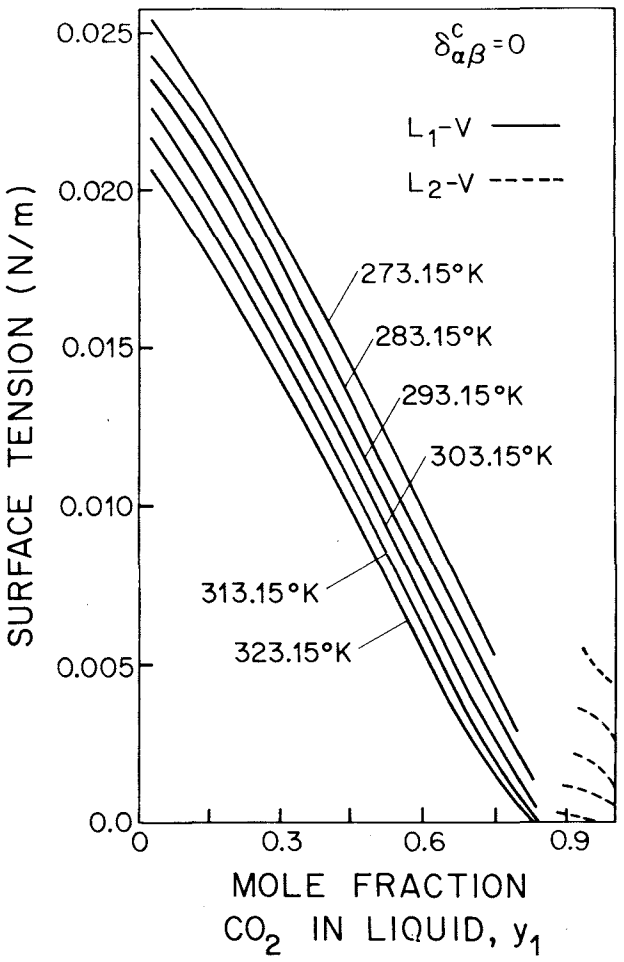

Fig. 19—Liquid-vapor surface tension-composition isotherms for CO_2-decane mixtures.

parameters $\delta^a_{\alpha\beta}$ and $\delta^c_{\alpha\beta}$ are similarly related to the interaction potential between molecules. It is reasonable from their analysis to expect $\delta^a_{\alpha\beta}$ and $\delta^c_{\alpha\beta}$ to be of similar magnitudes. Thus, since $\delta^a_{\alpha\beta}$ is about 0.1 for CO_2 with either C_3 or C_{10}, we expect $\delta^c_{\alpha\beta}$ to be about 0.1 for these pairs. Accordingly, in the calculations to follow, $\delta^c_{\alpha\beta}$ is set to zero for the C_3-C_{10} pair and equal to 0, 0.01, 0.05, or 0.1 for the CO_2-alkane pairs. We expect this range of parameters to span the values that are likely to be found for $\delta^c_{\alpha\beta}$ once experimental data are available for evaluating it. For reasons of thermodynamic stability, $\delta^c_{\alpha\beta}$ cannot be negative.[14]

Binary Mixtures. The most interesting tension behavior is that of CO_2-C_{10} mixtures. In Fig. 18A, the liquid-vapor tension predicted with $\delta^c_{\alpha\beta}=0$ is plotted vs. pressure at several temperatures. The trends in Fig. 18 can be understood by referring to the phase behavior summarized in Fig. 8. At 273.15 K [0°C], the L_2-V binodal approaches a critical point as pressure rises and tension consequently falls. The critical point is never reached because the L_2-V binodal is truncated by the splitting out of a second liquid phase at 3354 kPa [486.4 psi]. At the L_1-L_2-V equilibrium point there are three tensions, namely those of the L_1-V, L_2-V, and L_1-L_2 interfaces. At the phase equilibrium point at 273.15 K [0°C], the tension between the L_1 and V phases differs appreciably from that between the L_2 and V phases. The liquid-vapor tension changes discontinuously with pressure as the three-phase equilibrium point is passed, a behavior reflecting the fact that a different liquid phase is involved in the liquid-vapor equilibria above and below the three-phase equilibrium point.

With increasing temperature the two liquid phases at the three-phase equilibrium point approach a critical point. Indeed, at 293.15 K [20°C] the tensions of the L_2-V and L_1-V interfaces are very close at the three-phase point on the tension-pressure isotherms in Fig. 18, and by 303.15 K [30°C] the surface tension at the upper pressure of the L_1-V binodal is almost zero. At 323.15 K [50°C], the L_1-L_2 and L_2-V binodals are separated (Fig. 8C) and the

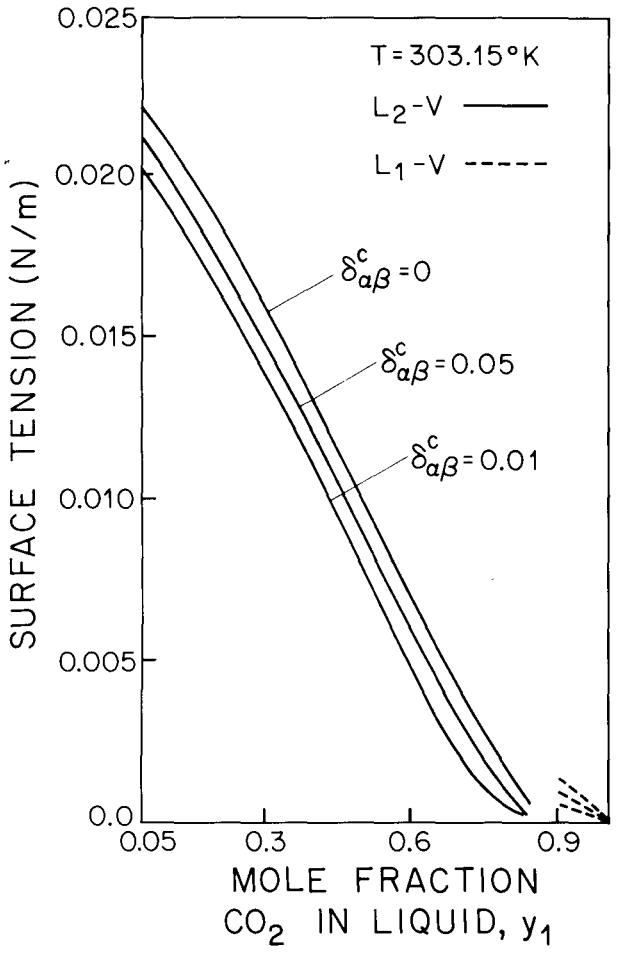

Fig. 20—Sensitivity of liquid-vapor surface tension of CO_2-decane mixtures of $\delta^c_{\alpha\beta}$.

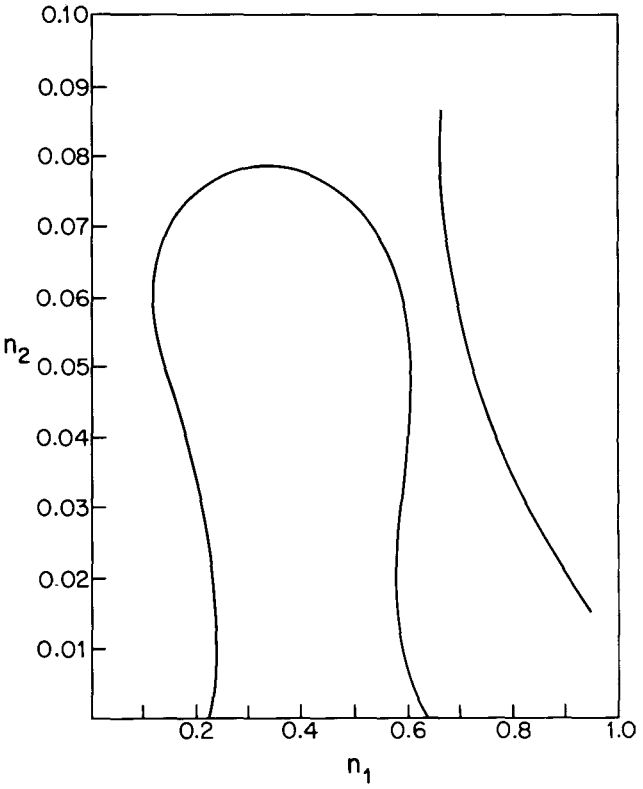

Fig. 21—Liquid-liquid discontinuous density profile for $\delta^c_{\alpha\beta} = 0$.

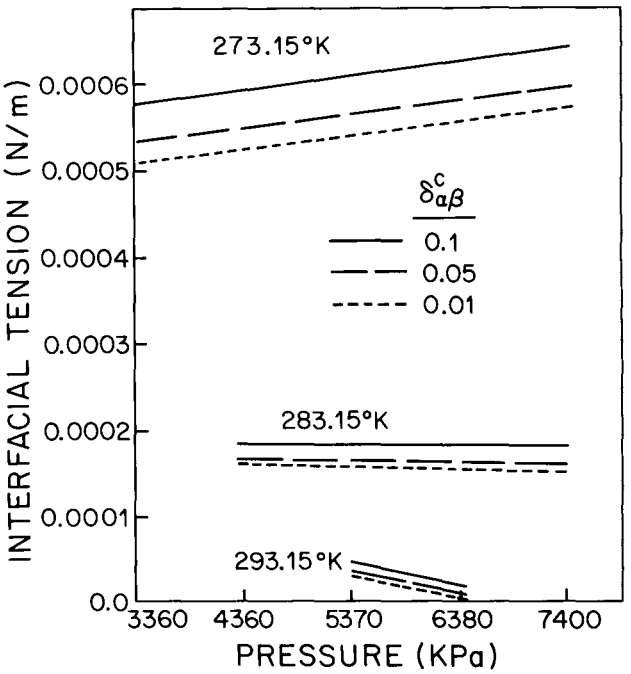

Fig. 22—Liquid-liquid interfacial tension-pressure isotherms for CO_2-decane mixtures.

L_2-V binodal ends in an upper critical pressure, at which point the tension is, of course, zero.

The intersection of the tension-pressure isotherms reflects the fact that the critical pressure of the L_2-V binodal (or the inferred critical pressure when the binodal is truncated by the L_1-L_2-V phase equilibria) increases with increasing temperature. Thus, the pressure range of the L_1-V isotherm is stretched out and orders the tensions as $\sigma(T_1) > \sigma(T_2)$ if $T_1 > T_2$ at high pressure. On the other hand, at very low pressures, the ordering of the surface tensions is the usual one: $\sigma(T_1) < \sigma(T_2)$ if $T_1 > T_2$.

Another way to display the liquid-vapor surface tension of CO_2 and C_{10} is to plot tension-composition isotherms as shown in Fig. 19. The isotherms are placed more simply relative to one another than are those in the tension-pressure coordinates. The sensitivity to the value chosen for $\delta^c_{\alpha\beta}$ is indicated in Fig. 20, where liquid-vapor surface tension is plotted vs. mole fraction y_1 of CO_2 in the liquid phase. Predictions with $\delta^c_{\alpha\beta} = 0$ are about 10% higher than those with $\delta^c_{\alpha\beta} = 0.1$ at low mole fractions. However, with increasing mole fraction and consequent decreasing tension, the percent error increases somewhat, a result implying the need for accurate values of $\delta^c_{\alpha\beta}$ if accurate low tension predictions are demanded. The qualitative trends are the same for all $\delta^c_{\alpha\beta}$ values used.

In computing liquid-liquid tensions for CO_2 and C_{10} with $\delta^c_{\alpha\beta} = 0$, a problem was encountered: the predicted density profile was discontinuous. The dependence of the

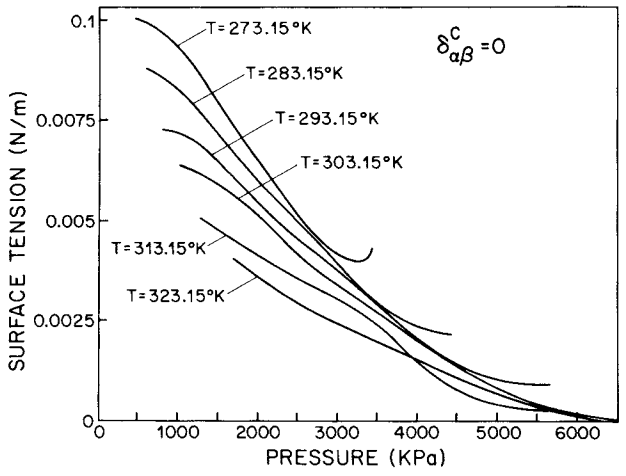

Fig. 23—Surface tension-pressure isotherms for CO_2-propane mixtures.

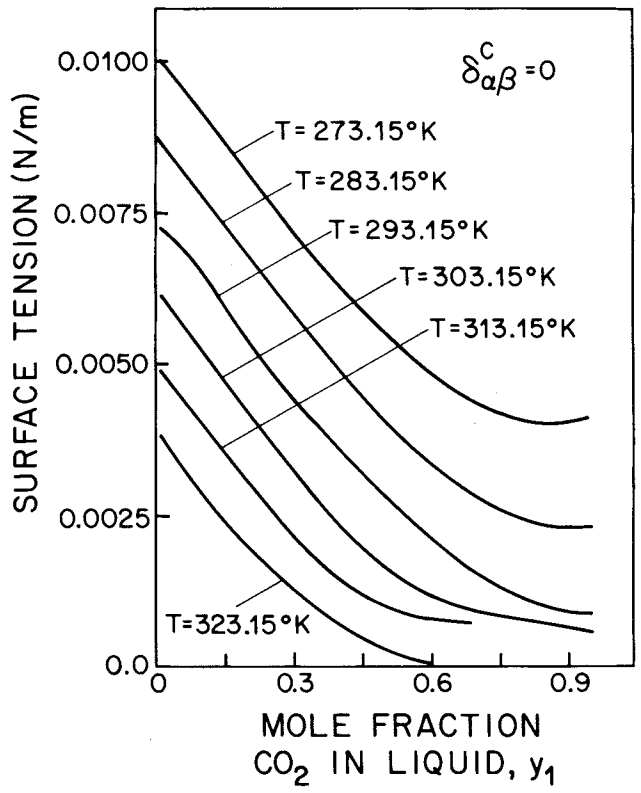

Fig. 24—Surface tension-composition isotherms for CO_2-propane mixtures.

density n_1 of CO_2 in the interfacial zone was determined by Eq. 14, which gradient theory gives when $\delta^c_{\alpha\beta}=0$. The result for a liquid-liquid interface at 273.15 K [0°C] is shown in Fig. 21. Mathematically, the discontinuous interfacial profile was avoided by setting $\delta^c_{\alpha\beta}$ equal to a small positive value; any small value would do because the liquid-liquid tension converges as $\delta^c_{\alpha\beta}$ goes to zero. Thus, although the CO_2-C_{10} interface becomes discontinuous in that limit, the tension remains well behaved. The discontinuous profile represents a weak solution of

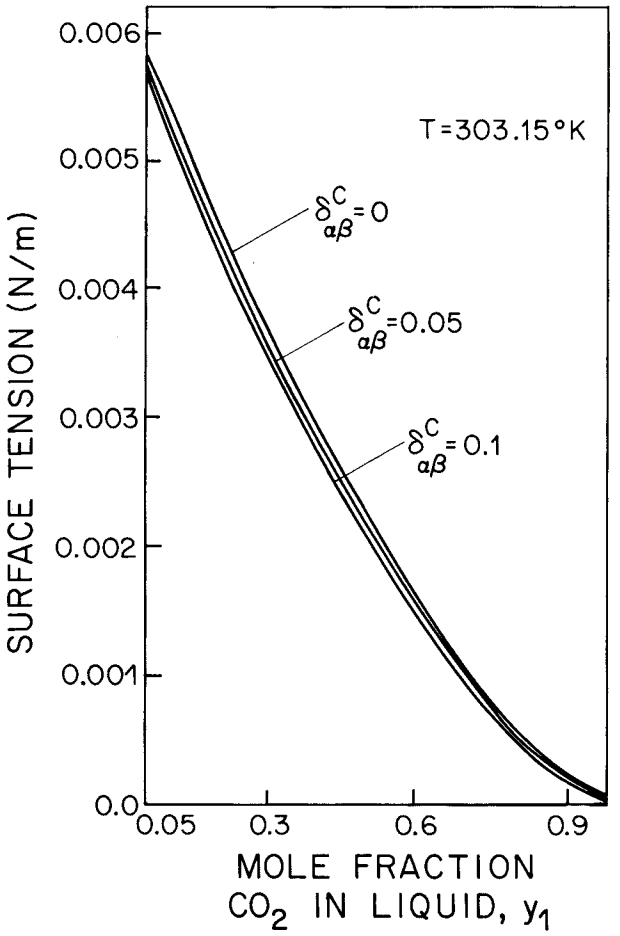

Fig. 25—Sensitivity of surface tension of CO_2-propane mixtures to $\delta^c_{\alpha\beta}$.

the gradient equation and may be an artifact of setting $\delta^c_{\alpha\beta}=0$ or, perhaps, of replacing rigorous integral equations by approximate differential ones,[20] a matter still under investigation. The artifact did not intrude because we computed the liquid-liquid tension of CO_2 and C_{10} with $\delta^c_{\alpha\beta}=0.01$, 0.05, and 0.1. (The discontinuity did not arise in cases of liquid-vapor interfaces, and the surface tensions predicted with $\delta^c_{\alpha\beta}=0.01$ are within 1% of those predicted with $\delta^c_{\alpha\beta}=0$.) Isotherms of liquid-liquid IFT vs. pressure appear in Fig. 22. The tension is a weak linear function of pressure and varies with $\delta^c_{\alpha\beta}$ about as strongly as does the liquid-vapor tension. The liquid-liquid tension increases with increasing $\delta^c_{\alpha\beta}$. The three tensions between pairs of the three L_1-L_2-V equilibrium phases are of special interest in connection with the phenomenon of wetting transition.[46-50]

Liquid-vapor tension-pressure and tension-mole fraction isotherms are given in Figs. 23 and 24 for CO_2-C_3 mixtures when the mixing parameter is set to zero—i.e., $\delta^c_{\alpha\beta}=0$. With rising pressure, the tension falls monotonically for most isotherms shown. However, the tension undergoes a change in curvature as pressure increases from the saturated vapor pressure of C_3 to that of CO_2. The 273.15 K [0°C] isotherm actually goes through a minimum and increases with pressure near the saturated vapor pressure of CO_2. The 273.15 K [0°C]

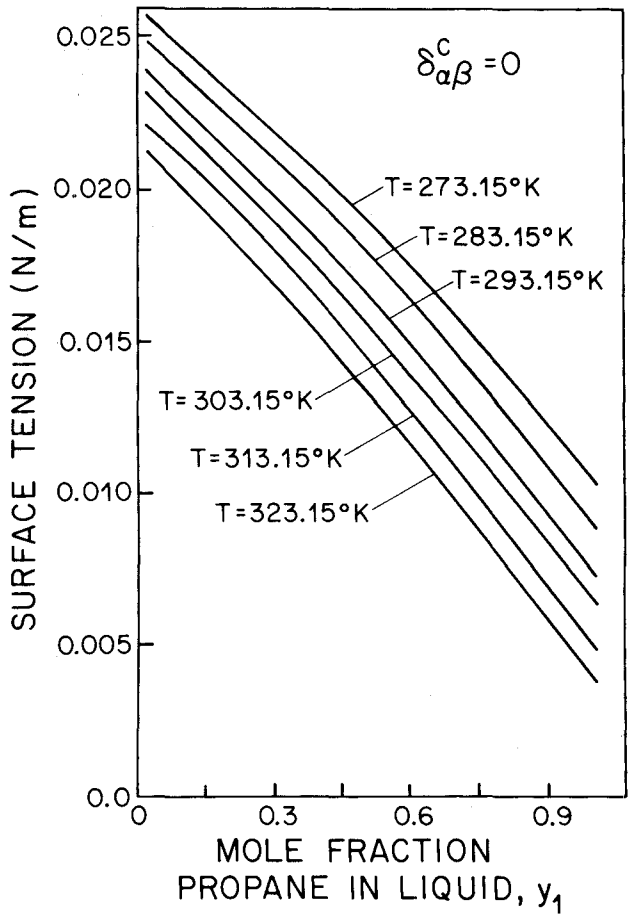

Fig. 26—Surface tension-composition isotherms for propane-decane.

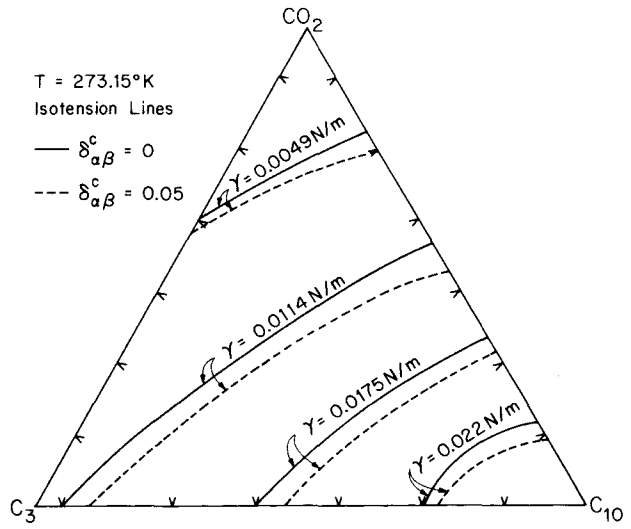

Fig. 27—Ternary diagrams of liquid-vapor isotension curves for CO_2-propane-decane mixtures at 273.15 K [0°C].

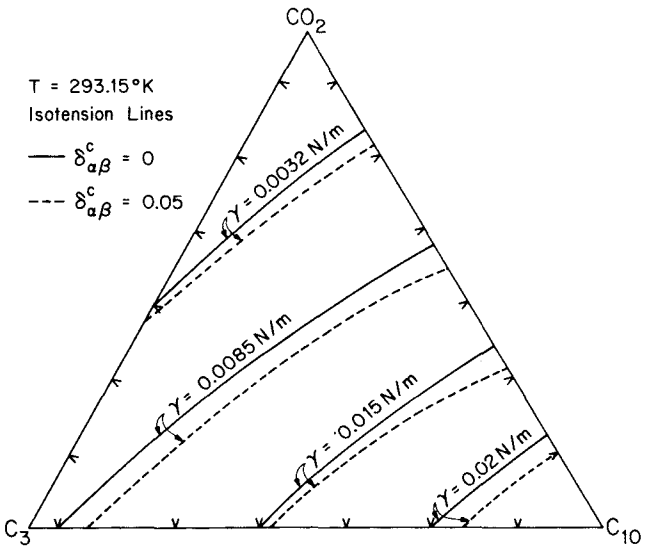

Fig. 28—Ternary diagrams of liquid-vapor isotherm curves for CO_2-propane-decane mixtures at 293.15 K [20°C].

isotherm of tension vs. mole fraction similarly goes through a minimum as pure CO_2 is approached.

As illustrated by Fig. 25, the surface tension of the CO_2-C_3 interface is as sensitive to $\delta^c_{\alpha\beta}$ as is that of the CO_2-C_{10} liquid-vapor interface. The $\delta^c_{\alpha\beta}=0$ and the $\delta^c_{\alpha\beta}=0.1$ isotherms differ by no more than 1% at the same mole fraction. The tension of the C_3-C_{10} liquid-vapor interface is given as a function of liquid phase composition in Fig. 26 for $\delta^c_{\alpha\beta}=0$. Carey *et al.*[24] have shown previously that gradient theory is accurate to within a few percent for normal alkanes with this mixing rule, and so no other value of $\delta^c_{\alpha\beta}$ was tested for the C_3-C_{10} mixture.

Ternary Mixtures. If the temperature and two mole fractions are set, the system is completely specified. The liquid-vapor tensions of the CO_2-C_3-C_{10} system were computed at the set of mole fractions at 273.15 K [0°C] and 293.15 K [20°C], with $\delta^c_{\alpha\beta}$ equal to zero for C_3-C_{10} and 0.05 for the CO_2-alkane pairs. From these calculations, the isotension curves shown in Figs. 27 and 28 were plotted. The curves illustrate the regularity of the composition dependence of tension at a fixed temperature and provide a measure of the sensitivity of tension to the value of $\delta^c_{\alpha\beta}$ for the CO_2-alkane pairs. Over much of each ternary diagram in Figs. 27 and 28 the ternary surface tensions are well approximated by the simple ideal mixture formula

$$\sigma=\sum_{i=1}^{3} y_i\sigma_i^0, \quad \ldots\ldots\ldots\ldots\ldots\ldots\ldots\ldots (33)$$

where σ_i^0 is the pure component surface tension of i and y_i is the liquid-phase mole fraction of i. Though this is quite accurate for all three pairs of binaries when $\delta^c_{\alpha\beta}=0$, it fails as $\delta^c_{\alpha\beta}$ is increased and the tension falls. Since pressure is not set, Figs. 27 and 28 are not easy to use; pressure is one of the independent variables. In such a case, predictions of tension vs. pressure at different compositions and temperatures are more convenient. Such predictions are given in Figs. 29 and 30 for $\delta^c_{\alpha\beta}=0$. It is interesting that the tension goes from a decreasing function of pressure to an increasing one as the concentration of CO_2 is increased.

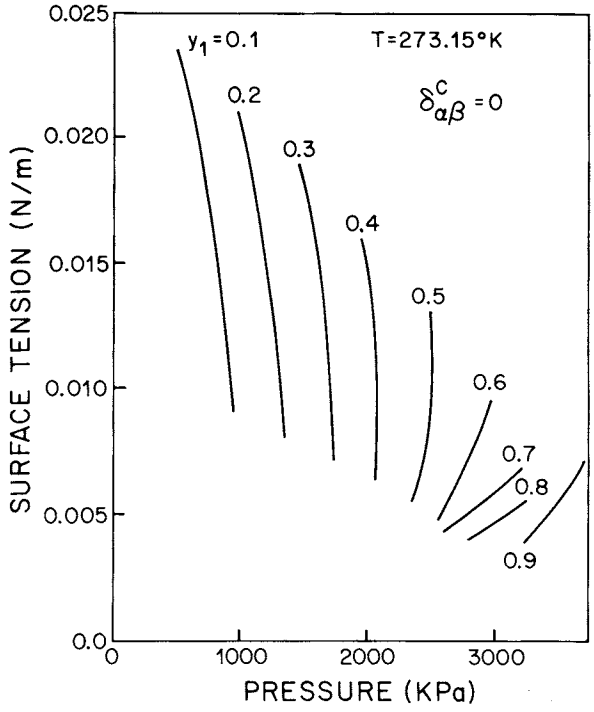

Fig. 29—Liquid-vapor surface tension vs. pressure for CO_2-propane-decane mixtures at 273.15 K [0°C].

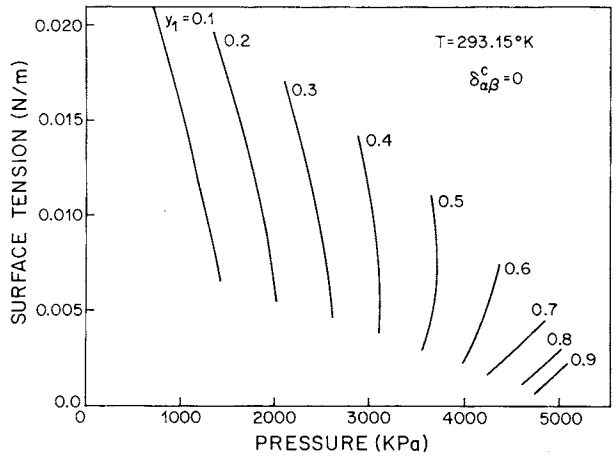

Fig. 30—Liquid-vapor surface tension vs. pressure for CO_2-propane-decane mixtures at 293.15 K [20°C].

Liquid-liquid tension for $\delta^c_{\alpha\beta}=0.01$ and 0.05 for CO_2-alkane binaries and $\delta^c_{\alpha\beta}=0$ for C_3-C_{10} are shown in Fig. 31 as functions of pressure at different mole fraction of C_3 in the L_2 liquid phase. The tensions are remarkably linear in pressure, as in the case of CO_2-C_{10} liquid-liquid tension. The idealization (Eq. 33) predicted for the liquid-vapor tension suggests simple approximations that the experimentalist might use to extrapolate data.

Conclusions

Given an EOS of homogeneous fluid and a set of influence parameters of inhomogeneous fluid, gradient theory provides a unified theory for predicting the phase behavior and IFT of multicomponent fluids. Influence parameters

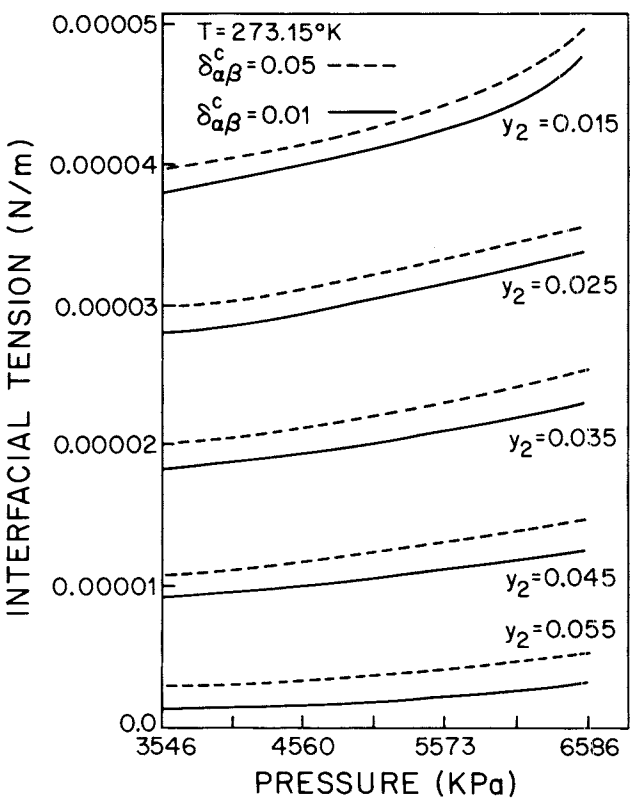

Fig. 31—Liquid-liquid IFT vs. pressure for CO_2-propane-decane mixtures at 273.15 K [0°C].

can be estimated from mixing rules in analogy with the mixing rules of the energy parameters in EOS or, preferably, from fits of theoretical to experimental tensions of binary mixtures.

Using the PREOS as a convenient illustrative model, we outline an efficient and systematic computational scheme to determine the phase behavior of multicomponent mixtures. In this scheme, the N-component phase diagram is found by continuation of features present in the related $N-1$-component phase diagrams and by computation of spinodal loci and critical points in the N-component system.

As applications, we map out the phase and tension behavior of binary and ternary mixtures of CO_2, C_3, and C_{10} in the temperature range pertinent to most oil reservoirs. The PREOS correctly predicts all the known qualitative patterns of phase behavior of these systems but fails to give good composition predictions in many cases and yields poor liquid densities even for one-component fluids. In separate papers,[51,52] the performance of the PREOS has been compared with that of a lattice gas model for systems of CO_2, water, and hydrocarbons.

The sensitivity of the tension predictions to choice of influence parameters indicates the necessity to have accurate estimates of these parameters and, therefore, points to the great need to enlarge substantially the IFT data base in binary systems.

The computational algorithm was designed for ease of incorporation into CO_2-flooding simulators whose phase behavior is handled by EOS. Thus, the simulator not only would locate regions of miscibility and phase splits but also would identify the low and high IFT regions.

Acknowledgments

This research was supported by grants from the U.S. DOE and the U. of Minnesota Computer Center. We are grateful to B.S. Carey for useful discussions in the early stage of this study, and to R.E. Benner for calling literature on the inverse iteration method to our attention.

Nomenclature

a = energy parameter of the EOS
a_m = energy parameter of mixture
$a_{\alpha\beta}$ = energy parameter of components α and β
a_{11} = energy parameter of component 1
a_{12} = energy parameter of components 1 and 2
b = volume parameter of the EOS
b_1 = volume parameter of component 1
c = influence parameter matrix
$c_{\alpha\alpha}$ = interfacial influence parameter of component α
$c_{\alpha\beta}$ = interfacial influence parameter of components α and β
f^0 = Helmholtz free energy density of homogeneous fluid
F = defined by right side of Eq. 10
F_α = αth component of F
H = Hessian energy matrix
J = determinant of H
k = Boltzmann's constant
$\boldsymbol{n}$ = set of component densities $n_1 \ldots n_\nu$
n_i = density of component i
n_i^α = density of component i in phase α
$\boldsymbol{n}^L$ = set of component densities in liquid phase
$\boldsymbol{n}^V$ = set of component densities in vapor phase
n_α^L = density of component α in liquid phase
n_α^V = density of component α in vapor phase
p = set pressure
p^0 = pressure of homogeneous fluid
r^α = relaxation parameter of phase α
T = absolute temperature
$T_{R\alpha}$ = reduced temperature of component α
x = position in interfacial zone
x_i^L = mole fraction of component i in liquid phase
y = mole fraction
y_i^α = mole fraction of component i in phase α
y_α = mole fraction of component α
$\delta_{\alpha\beta}^a$ = adjustable energy (interaction) parameter
$\delta_{\alpha\beta}^c$ = influence parameter scaling parameter
ϵ = residual value
μ_α = chemical potential of component α
μ_α^0 = chemical potential of component α in homogeneous fluid at composition n
ν = number of component
σ = interfacial tension
Φ_B = bulk thermodynamic potential
$\Phi(\boldsymbol{n})$ = thermodynamic potential
$\Delta\Phi(\boldsymbol{n})$ = thermodynamic potential difference
ω_a = acentric factor of component α
ω_B = bulk phase thermodynamic potential

References

1. Holm, L.W.: "Status of CO_2 and Hydrocarbon Miscible Oil Recovery Methods," *J. Pet. Tech.* (Jan. 1976) 76–84.
2. Holm, L.W. and O'Brian, L.J.: "Carbon Dioxide Test at the Mead-Strawn Field," *J. Pet. Tech.* (April 1971) 431–42.
3. Holm, L.W.: "A Comparison of Propane and CO_2 Solvent Flooding Processes," *AIChE J.* (1961) **7**, 179–84.
4. Holm, L.W.: "Carbon Dioxide Solvent Flooding for Increased Oil Recovery," *J. Pet. Tech.* (Sept. 1959) 225–31; *Trans.*, AIME, **216**.
5. Holm, L.W. and Josendal, V.A.: "Mechanisms of Oil Displacement by Carbon Dioxide," *J. Pet. Tech.* (Dec. 1974) 1427–38; *Trans.*, AIME, **257**.
6. Simon, R., Rosman, A., and Zana, E.: "Phase-Behavior Properties of CO_2-Reservoir Oil Systems," *Soc. Pet. Eng. J.* (Feb. 1978) 20–26.
7. Shelton, J.L. and Yarborough, L.: "Multiple Phase Behavior in Porous Media During CO_2 or Rich-Gas Flooding," *J. Pet. Tech.* (Sept. 1977) 1171–78.
8. Hutchinson, C.A. Jr. and Braun, P.H.: "Phase Relationship of Miscible Displacement in Oil Recovery," *AIChE J.* (1961) **7**, 65–72.
9. Metcalfe, R.S. and Yarborough, L.: "The Effect of Phase Equilibria on the CO_2 Displacement Mechanism," *Soc. Pet. Eng. J.* (Aug. 1979) 242–52.
10. Rathmell, J.J., Stalkup, F.I., and Hassinger, R.C.: "A Laboratory Investigation of Miscible Displacement by CO_2," paper SPE 3483 presented at the 1971 SPE Annual Meeting, New Orleans, Oct. 3–6.
11. Peng, D.Y. and Robinson, D.B.: "A New Two-Constant Equation of State," *Ind. Eng. Chem. Fund.* (1976) **15**, 59–64.
12. Soave, G.: "Equilibrium Constants From a Modified Redlich-Kwong Equation of State," *Chem. Eng. Sci.* (1972) **27**, 1197–1203.
13. Redlich, O.V. and Kwong, J.N.S.: "On the Thermodynamics of Solutions: An Equation of State," *Chem. Rev.* (1949) **44**, 233–40.
14. Carey, B.S.: "The Gradient Theory of Fluid Interfaces," PhD dissertation, U. of Minnesota, Minneapolis (1979).
15. Orr, F.M. Jr., Lien, C.L., and Pelletier, M.T.: "Liquid-Liquid Phase Behavior in CO_2-Hydrocarbon Systems," paper presented before the Div. of Petroleum Chemistry Inc., American Chemical Soc., Atlanta, March 29–April 3, 1981.
16. Heidemann, R.A. and Khalil, A.M.: "The Calculations of Critical Points," *AIChE J.* (1980) **26**, 769–79.
17. Michelsen, M.L.: "Calculation of Phase Envelopes and Critical Points for Multicomponent Mixtures," *Fluid Phase Equil.* (1980) **4**, 7–70.
18. Michelsen, M.L. and Heidemann, R.A.: "Calculation of Critical Points From Cubic Two-Constant Equation of State," *AIChE J.* (1981) **27**, 521–23.
19. Sahimi, M.: "Transport and Dispersion in Porous Media and Related Aspects of Petroleum Recovery," PhD dissertation, U. of Minnesota, Minneapolis (1984).
20. Davis, H.T. and Scriven, L.E.: "Stress and Structure in Fluid Interfaces," *Adv. Chem. Phys.* (1982) **49**, 357–454.
21. Bongiorno, V., Scriven, L.E., and Davis, H.T.: "Molecular Theory of Fluid Interfaces," *J. Colloid and Interface Sci.* (1976) **57**, 462–75.
22. Fleming, P.D. III, Yang, A.J.M., and Gibbs, J.H.: "A Molecular Theory of Interfacial Phenomena in Multicomponent Systems," *J. Chem. Phys.* (1976) **65**, 7–17.
23. McCoy, B.F. and Davis, H.T.: "Free-Energy Theory of Inhomogeneous Fluids," *Phys. Rev. A.* (1979) **20**, 1201–07.
24. Carey, B.S., Scriven, L.E., and Davis, H.T.: "Semiempirical Theory of Surface Tensions of Binary Systems," *AIChE J.* (1980) **26**, 705–11.
25. Benedict, M., Webb, G.B., and Rubin, L.C.: "An Empirical Equation for Thermodynamic Properties of Light Hydrocarbons and Their Mixtures," *J. Chem. Phys.* (1940) **8**, 334–45.
26. Prausnitz, J.M. *et al.*: *Computer Calculations for Multicomponent Vapor-Liquid and Liquid-Liquid Equilibria*, Prentice-Hall Inc., Englewood Cliffs, NJ (1980) 110.
27. Doring R. and Knapp, H.: *In Phase Equilibria and Fluid Properties in the Chemical Industry*, DECHEMA, Frankfurt/Main, Federal Republic of Germany (1980) 127.
28. Mohanty, K.K., Dombrowski, M., and Davis, H.T.: "Comparison of a Pair of Three Parameter Equations of State," *Chem. Eng. Commun.* (1980) **5**, 85–91.
29. Leder, F. and Irani, C.A.: "Upper Critical Solution Temperatures in Carbon Dioxide-Hydrocarbon Systems," *J. Chem. Eng. Data* (1975) **20**, 323–27.

30. Orr, F.M. Jr., Yu, A.D., and Lien, C.L.: "Phase Behavior of CO_2 and Crude Oil in Low-Temperature Reservoirs, *Soc. Pet. Eng. J.* (Aug. 1981) 480–92.
31. Reamer, H.H., Sage, B.H., and Lacey, W.N.: "Phase Equilibria in Hydrocarbon Systems: Volumetric and Phase Behavior of the Propane-Carbon Dioxide System," *Ind. Eng. Chem.* (1951) **43**, 2515–20.
32. Poettmann, F.H. and Katz, D.L.: "Phase Behavior of Binary Carbon Dioxide-Paraffin Systems," *Ind. Eng. Chem.* (1945) **37**, 847–53.
33. Meldrum, A.H. and Nielsen, R.F.: "A Study of Three-Phase Equilibria for Carbon Dioxide and Several Normal Saturated Hydrocarbons," *Prod. Monthly* (Jan. 1954) 27–32.
34. Stewart, W.C. and Nielsen, R.F.: "Phase Equilibria for Mixtures of Carbon Dioxide and Several Normal Saturated Hydrocarbons," *Prod. Monthly* (Jan. 1954) 27–32.
35. Reamer, H.H. and Sage, B.H.: "Phase Equilibria in Hydrocarbon Systems: Volumetric and Phase Behavior of the n-Decane-CO_2 System," *J. Chem. Eng. Data* (1963) **8**, 508–13.
36. Schneider, G. *et al.*: "Phasengleichgewichte und kritische Erscheinungen in binarden Mischsystemen bis 1500 bar: CO_2 mit n-Octan, n-Undecan, n-Tridecan, und n-Hexadecan," *Chem. Ing. Tech.* (1967) **39**, 649–56.
37. Zarah, B.Y., Luks, K.D., and Kohn, J.P.: "Phase Equilibria Behavior of Carbon Dioxide in Binary and Ternary Systems with Several Hydrocarbon Components," *AIChE Symposium Series* (1974) **70**, No. 140, 91–101.
38. Kulkarni, A.A. *et al.*: "Phase Equilibria Behavior of Carbon Dioxide-n-Decane at Low Temperatures," *J. Chem. Eng. Data* (1974) **19**, 92–94.
39. Hule, N.C., Luks, K.D., and Kohn, J.P.: "Phase Equilibria Behavior of Systems of CO_2-n-Eicosane and CO_2-n-Decane-Eicosane," *J. Chem. Eng. Data* (1973) **18**, 311–13.
40. Yang, H.W., Luks, K.D., and Kohn, J.P.: "Phase Equilibria Behavior of the System CO_2-n-Butylbenzene-2-Methylnaphthalene," *J. Chem. Eng. Data* (1976) **21**, 330–35.
41. Francis, A.W.: "Ternary Systems of Liquid Carbon Dioxide," *J. Phys. Chem.* (1954) **58**, 1099–1114.
42. Francis, A.W.: "Solvent Extraction with Liquid Carbon Dioxide," *Ind. Eng. Chem.* (1955) **47**, 230–33.
43. Rosman, A. and Zana, E.: "Experimental Studies of Low Interfacial Tension Displacement by CO_2 Injection," paper SPE 6723 presented at the 1977 SPE Annual Technical Conference and Exhibition, Denver, Oct. 9–12.
44. Brauer, E.B. and Hough, E.W.: "Interfacial Tension of the Normal Butane-Carbon Dioxide System," *Prod. Monthly* (1965) **29**, 13.
45. Carey, B.S., Scriven, L.E., and Davis, H.T.: "Semiempirical Theory of Surface Tension of Pure Normal Alkanes and Alcohols," *AIChE J.* (1978) **24**, 1076–80.
46. Pujado, P.R. and Scriven, L.E.: "Sessile Lenticular Configurations: Translationally and Rotationally Symmetric Lenses," *J. Colloid and Interface Sci.* (1972) **40**, 82–98.
47. Cahn, J.W.: "Critical-Point Wetting," *J. Chem. Phys.* (1977) **66**, 3667–72.
48. Teletzke, G.F., Davis, H.T., and Scriven, L.E.: "How Liquids Spread on Solids," paper presented at the 1981 AIChE Annual Meeting, New Orleans, Nov. 8–12.
49. Teletzke, G.F., Scriven, L.E., and Davis, H.T.: "Patterns of Wetting in Multicomponent Systems," paper SPE 10112 presented at the 1981 SPE Annual Technical Conference and Exhibition, San Antonio, Oct. 5–7.
50. Widom, B.: "Antonov's Rule and the Structure of Interfaces Near Tricritical Points," *Phys. Rev. Letter* (1975) **34**, 999–1002.
51. Kuan, D.-Y. *et al.*: "Multicomponent Carbon Dioxide/Water/Hydrocarbon Phase Behavior Modeling: A Comparative Study," paper SPE 11961 presented at the 1983 SPE Annual Technical Conference and Exhibition, San Francisco, Oct. 5–8.
52. Nitsche, J.M. *et al.*: "Phase Behavior of Binary Mixtures of Water, Carbon Dioxide, and Decane Predicted With a Lattice-Gas Model," *Fluid Phase Equilibria* (1984) **17**, 243–63.
53. Reid, R.C., Prausnitz, J.M., and Sherwood, T.K.: *The Properties of Gases and Liquids*, McGraw-Hill Book Co., New York City (1977) 629.

SI Metric Conversion Factors

cu ft	× 2.831 685	E−02	= m^3
ft	× 3.048*	E−01	= m
°F	(°F−32)/1.8		= °C
°F	(°F+459.67)/1.8		= K
lbf	× 4.448 222		= N

*Conversion factor is exact.

SPEJ

Original manuscript received in the Society of Petroleum Engineers office Sept. 15, 1981. Paper accepted for publication Aug. 19, 1983. Revised manuscript received Nov. 14, 1984. Paper (SPE 10268) first presented at the 1981 SPE Annual Technical Conference and Exhibition held in San Antonio Oct. 5–7.